Surface Variation Characterization and Control Using High-Definition Metrology

by

Hai Trong Nguyen

A dissertation submitted in partial fulfillment
of the requirements for the degree of
Doctor of Philosophy
(Mechanical Engineering)
In the University of Michigan
2013

Doctoral Committee:

Professor S. Jack Hu, Co-Chair
Research Scientist Hui Wang, Co-Chair
Assistant Professor Eunshin Byon
Professor Elijah Kannatey-Asibu Jr.

ACKNOWLEDGEMENTS

I would like to thank my advisor, Professor Jack Hu, for recruiting me to Michigan and providing me an opportunity to do research in his group under his mentorship. He not only gave me profound professional guidance but also has been very patient and flexible to give me time and space for personal growth. The time I spent working with him and his group is an unforgettable period of time in my life: I have learned a lot during this period of time.

I also would like to thank my co-advisor, Dr. Hui Wang, for his enthusiastic guidance and support in doing research. He spent significant amount of time discussing and improving my research. He is also my good friend who shares with me knowledge besides research.

I also would like to thank all my committee members for all their advice and suggestions about my research. Their knowledge from other points of view helps me improve my research quality.

I would like to thank all the group members in the Hu lab for their help and support, the great insights and valuable discussions.

I would like to thank my friends who support and make my life during PhD study more enjoyable.

Most importantly, I would like to thank my family for their love and support. I would like to thank my parents and my sister for always believing in me.

TABLE OF CONTENTS

LIST OF FIGURES

LIST OF TABLES

ABSTRACT

The surface shape of a machined part plays a significant role in affecting assembly performance. For example, surface variation on a deck face of a combustion engine block can impact the performance of the engine assembly, resulting in sealing problems and cam bore distortions. Control of such surface shape variation becomes a key enabler of high-precision machining and requires the characterization of surface shapes with fine lateral resolution. Past research on machined surface quality includes surface error characterization, flatness prediction, and error diagnosis. However, conventional metrology systems cannot capture the shape variation of large machined surfaces with sufficient lateral resolution due to the limited capability in measurement resolution and range.

Recently, a new type of surface measurement system based on laser holographic interferometry (LHI) is made available for high-definition surface metrology. Such a measurement system can reveal shape variations of a large surface with fine resolution, providing opportunity for surface variation characterization and control. Using the LHI, this dissertation develops models and algorithms for surface shape variation characterization and reduction. Based on face milling, three research topics are addressed in this dissertation:

1. *Characterization of surface variation induced by cutter-workpiece relative displacement*: The surface patterns are extracted by modeling the impacts of cutting force variation on relative cutter-workpiece displacements and correlating such displacement with LHI measurements.

2. *Characterization of surface variation induced by cutter-spindle deflection:* The cutting force variation due to part geometry also causes the cutter-spindle to deflect, resulting in the surface variation along the cutter path. This research investigates the impact of cutter-spindle deflection on surface variation and develops algorithms for machine tool health monitoring.
3. *Surface variation reduction:* Based on the extracted surface patterns and derived cutting force models, a machining method for surface variation reduction is developed by optimizing cutting conditions and cutter path to redistribute cutting force real time.

The research presented in this dissertation provides an in-depth understanding of the relationship between machined surface shape patterns and process conditions such as cutting forces and machine setup. The outcome of this research will lead to methodologies for cost-effective monitoring and control of surface variations.

CHAPTER 1

INTRODUCTION

1.1 Problem Statement

Surface shapes have a crucial impact on product functions. For example, in the automotive industry, surface shape variation surrounding the bores on a deck face of the head block an internal combustion engine may affect the sealing between the deck face and head gasket during the subsequent assembly. To capture these variation efficiently, metrology techniques that can scan large surfaces with micron-level resolution are needed. It has been difficult to precisely characterize the detailed surface shape using measurement devices employed in manufacturing plants today.

Various surface metrology techniques have been developed over the past several decades, including contact and noncontact techniques. The contact surface metrology uses a stylus, probe, or retroreflector to scan a surface. The non-contact metrology systems employ optical methods. Extensive reviews on these techniques are given by Huynh et al. [1] and Whitehouse [2].

The disadvantage of these techniques is a lack of efficiency in measuring large surfaces with high resolution. The conventional high resolution metrology systems have very limited scanning range and required long measurement time. For the contact metrology system, though the scanning range can be up to hundreds or thousands of millimeters, the contact mechanism usually requires significant amount of time in scanning large complex surfaces. Furthermore, the

tip size associates with certain contact scanning systems can lead to reduced lateral resolution, rendering it difficult to precisely obtain fine-scale surface information. The noncontact metrology system that can characterize a large area, such as an optical CMM, usually has a poor vertical resolution.

Recently, a new type of high-definition metrology (HDM) system has been developed to inspect surfaces with high resolution along the vertical and lateral directions. Such a system is capable of measuring large 3D surfaces using laser holographic interferometry (LHI) [3-4]. For example, within 1 to 2 minutes, it can collect 4-million data points from an area of up to $300\times300mm^2$. Figure 1-1 qualitatively compares the inspection range and lateral resolutions between LHI based HDM and common in-plant surface gages such as CMM and conventional HDM such as 3D stylus-based profilometer, optical profilometer, 3D-microscope [5]. It can be seen that the LHI system achieves a 150 μm lateral resolution at a relatively high scanning speed. As such, it offers measurement capability that fills the gap between profilometer and CMM.

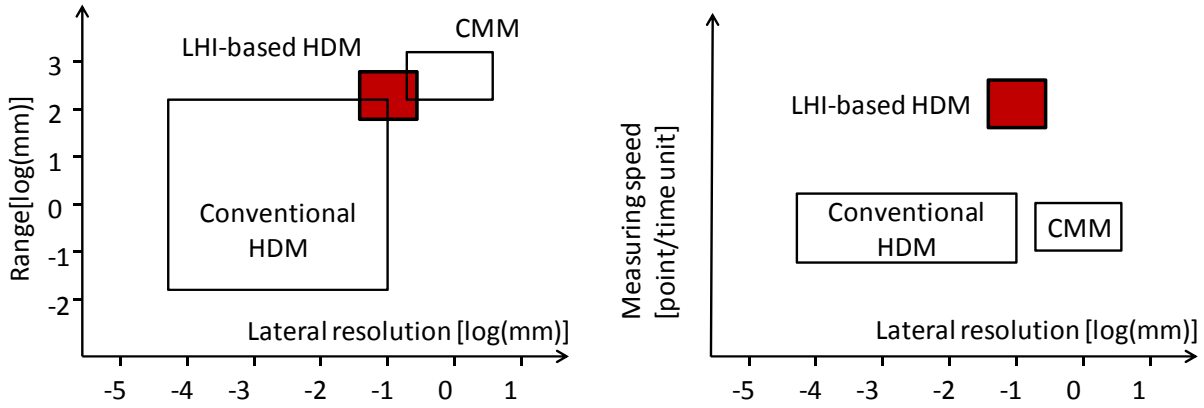

Figure 1-1 Comparison among LHI-based HDM, conventional HDM, and CMM in plants: (a) Measurement range, (b) Measurement speed

Figure 1-2 shows the HDM image of a deck face on an engine head. The aforementioned surface height variation surrounding the cylinder bores can be clearly observed. These surface distortions can be captured at multiple length scales, from millimeters to decimeters, depending on the workpiece size as well as the cutter geometry. Such HDM presents new opportunities for the understanding the cutting process and improving quality in high-precision machining.

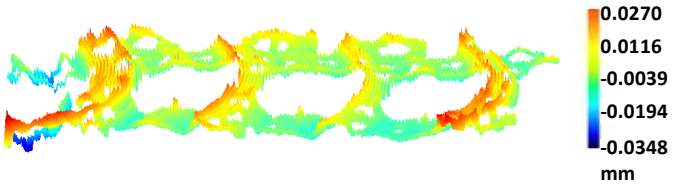

Figure 1-2 A face milled surface measured by the LHI

This dissertation aims to develop models and algorithms for the characterization and reduction of surface shape variation (Figure 1-3) by (1) conducting cutting force modeling to relate surface variation to cutting forces variation, and (2) developing algorithms to reduce surface variation by redistributing cutting forces variation. The methodology will be developed based the face milling process.

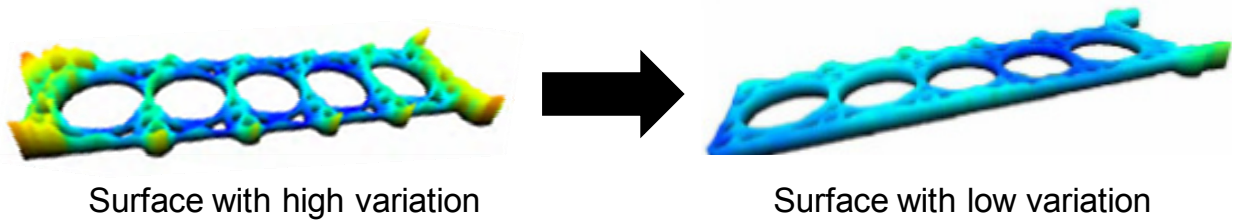

Figure 1-3 Surface variation reduction

1.2 Literature Review

This section reviews research related to face milling including surface characterization and analysis, surface prediction, surface quality monitoring and diagnosis, surface quality

improvement, as well as impacts of process conditions on surface variations such as the effects of structure of machine, kinetics (cutting conditions), cutting dynamics (cutting force, vibration), and workpiece material.

1.2.1 Mechanics of Cutting

Structural Components

In a face milling operation (Figure 1-4), the cutter rotates about a fixed axis of spindle and the inserts of the cutter in contact with workpiece surface remove material from the workpiece to obtain a planar surface. The workpiece is clamped on a fixture that is firmly fixed onto a moving table.

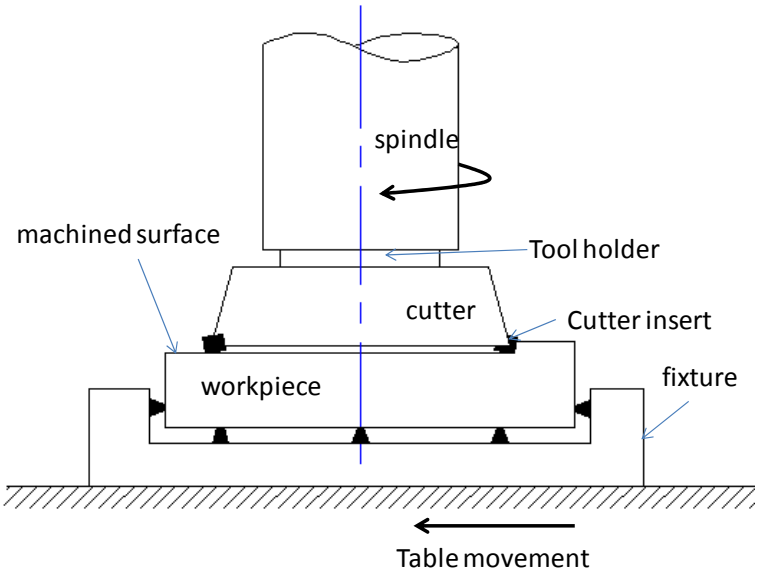

Figure 1-4 Face milling operation

The critical components in a machining process that impact surface quality include cutter-spindle assembly, cutter insert, workpiece, fixture, and machine table. This section briefly reviews the related study on each component.

Cutter-holder-spindle assembly: Poor design and operation of cutter-holder-spindle would produce self-excited vibration of the cutter resulting in unstable cutting process, poor surface finish, low productivity, and fast decaying of the machine tool. Design parameters such as spindle geometry, bearing stiffness, bearing locations and operational parameters such as holder/cutter structure, clamping force should be chosen carefully to make the system stable to avoid chatter [6]. Relative position of cutter-holder-spindle to workpiece also affects surface quality [7]. Other factors such as feed rate fluctuation, insert cutting edge, and the back-cutting may produce variation in surface finish [8]. Sastry et al. (1999) investigated geometrical errors such as spindle axis tilt, cutter axis tilt, and cutter center offset that result in radial and axial run-out on cutter inserts and chose an optimal value of spindle speed to compensate for the runouts to improves surface quality.

Cutter-Inserts: Insert runouts and the variation in axial/radial locations of inserts can impact surface topography, surface location error, and machining stability [9]. The runouts result in chip load variation and the varying chip load can cause permanent failure of cutting edges [10].

Workpiece Geometry: There is limited work on the impact of surface geometry on surface profile. Gu et al. (1997) studied the effects of surface features such as holes, slots [11] on the cutting force variation and resultant surface variation.

Fixture: A fixture is used to locate the workpiece position relative to the cutter and clamp the workpiece to avoid relative movement of workpiece to the machine table. The fixturing problems are related to fixture layout and clamping force. The fixture layout and force can be adjusted to

reduce the workpiece deformation. For example, the fixture layout can be designed to compensate for thermal deformations [12]. The fixture layout design and clamping force also can be optimized to minimize the effect of workpiece deformation [13-15]. The clamping forces were also determined for maintaining the dynamic stability of fixturing [16-17].

The Cutting Dynamics

Process variables related to motion of cutter and workpiece such as cutting speed and feed rate could affect surface finish, cutting force variation, vibration, and tool-chip contact length [18-19]; [20-21], and dynamic issues of cutting.

The dynamics of cutting process such as cutting forces and vibration always has drawn broad attentions. Research has been conducted on the effects of cutting forces and vibration on surface roughness, surface shape deformation of workpiece, deflection of cutter-spindle assembly and the performance of machine tool.

Cutting forces: Many studies established models to predict cutting forces and cutting force variation [22-28]. The change of real-time cutting forces during machining process was also studied since it can cause vibration, high rate of tool wear, and surface finish [29-31].

Vibration: The vibration can generate chatter patterns on the machined surface and reduce the tool life. The root cause is related to the dynamics of cutting processes including (1) the magnitude of cutting force determined by depth of cut, feed rate, cutter-insert geometry and (2) variation of cutting forces determined by cutting speed (spindle speed), cutter geometry and workpiece geometry. Research was also conducted to regulate spindle speed to stabilize the vibration and reduce the chatter [32-33].

Workpiece and Cutter Material

The material properties of workpiece such as residual stress and thermal expansion also significantly affect the machined surface variation. The thermal expansion of cutter and workpiece due to the heat generated during cutting can change the relative position between cutter and workpiece, making the machined surface undesirable [7, 34].

1.2.2 Surface Characterization

Surface Characterization and Analysis

A machined surface has been characterized by multi-scale features, including error of form, lay, waviness, and roughness [35]. The purpose of surface characterization is for monitoring and control of the machining process [1]. It can be used to monitor tool wear based on surface texture parameters [36-37] or vibration based on roughness [38].

Surface Prediction

Prediction of surface with given conditions of machine and cutting conditions is important to product and process designs. The surface can be predicted with consideration of cutting conditions, elastic deformation of cutter-spindle and workpiece-fixture assemblies, static spindle axis tilt, and axially inclined tool path [39]. The elastic deformation of cutter-spindle and workpiece-fixture assemblies at cutting points/areas can be estimated using equivalent flexibility, a finite element method. The finite element analysis also can be used to investigate the influence of clamping preload and machining force on the machined surface considering the effects of fixture and machine table compliance, workpiece and locators/clamps contact interaction, and

forced vibration [40]. Extensive studies have been conducted on surface roughness prediction. For example, surface roughness can be predicted using measured signals of spindle displacement [41].

1.2.3 Surface Variation Control

To improve the performance of precision parts and assemblies with machined surfaces, it is critical to improve surface quality such as flatness. A study was conducted [34] to improve form error of plate-shaped workpiece using clamping layouts. The study found positions to clamp the workpiece so that the clamping force induced elastic deformation is compensated for by thermal deformation caused by cutting heat. Surface flatness also can be improved by cutting depth compensation or by optimizing feed rate [42].

There are many factors that impact surface quality such as tool wear, tool breakage, fixture fault, vibration and therefore it is important to monitor and diagnose these factors. The process can be monitored and diagnosed by using direct and indirect methods. The indirect method uses signals measured from the machined surface such as surface profile while the direct method uses inline signals directly from processes such as cutting forces and vibration. For example, the tool wear can be recognized by measuring surface finish parameters [43] or by monitoring wear patterns in cutting force signal [44] or vibration signal [38]. The tool breakage can be diagnosed by measuring fluctuations in spindle rotational speed [45]. Methods also exist on detecting other factors that contribute to surface quality such as fixture error or cutter geometry errors. For example, process faults like radial runout, spindle tilt, dynamic cutter imbalance, and insert breakage can be detected by using model-based approach [46]. Fixture faults can be detected by using designated component analysis [47].

Research Gaps

Due to the limitations of measurement systems being used, there is a lack of

- *An understanding of surface variation patterns uncovered by HDM* (e.g., as shown in Fig. 1-2). Due to a lack of efficient HDM systems in the past, very limited research reported the patterns of local variations over a large surface. Prior data-driven characterization methods, such as spline surface, frequency domain approaches, and wavelet, fall short of extracting interpretable variation patterns for surface variation control.
- *An efficient method of process monitoring and diagnosis by surface inspection*. The surface variation patterns could contain rich information about machining processes. However, conventional methods mainly employ inline sensing systems to monitor and diagnose machine conditions such as machine tool setup and stiffness. Thus, new opportunities exist to develop efficient process monitoring and diagnosis based on routine surface quality inspection without having to interrupt normal production cycle.
- *A cost-effective method of variation reduction for large surfaces*. Surface height variation reduction has rarely been applied in large surface machining processes. Most of previous research focuses on real-time adjustment (e.g., adaptive control) of operating parameters related to machine tools, requiring additional installation of in-line sensors and control actuators. The surface patterns identified by HDM present new opportunities of developing a cost-effective method for surface variation control based on routine surface inspection.

1.3 Research Objectives and Thesis Organization

The goal of this research is to develop models and algorithms for surface shape variation characterization and control by:

1) Developing a method of extracting surface shape variation patterns by conducting cutting force modeling and HDM.
2) Developing algorithms of monitoring machine tool conditions by extracting process parameters/variables from surface patterns.
3) Optimizing machining conditions to reduce surface variations based on cutting force models and HDM.

This thesis is organized as shown in Figure 1-5. Chapter 2 studies the impact of cutter-workpiece relative displacement on surface shape by introducing a model that relates cutter-workpiece relative displacement to axial cutting forces. The model will help explain surface height variations along cutter path and circumferential directions. The model is validated by experimental data and data from a manufacturing plant.

Chapter 3 studies the impact of cutter-spindle deflection on surface shape and algorithms for process monitoring are also developed based on the extracted patterns. It also derives a model that relates cutter-spindle deflection to the moment of cutting forces. The model will help explain part of surface height variation along cutter path due to variation of cutter-spindle deflection. Case studies were conducted to validate the model. The surface height variation patterns found in both Chapter 2 and 3 are caused by the variation of cutting forces. The variation of cutting forces is mainly caused by the complexity of surface geometry that leads to the variation of material removal rate.

The findings in Chapter 2 and 3 are utilized to reduce surface variations in Chapter 4 by developingan approach to reduce the surface variation by redistributing cutting forces along cutter path and on both sides of cutter path. The methodology of surface variation reduction will potentially lead to cost-effective high-precision machining.

Chapter 5 summarizes the thesis and presents topics for future research.

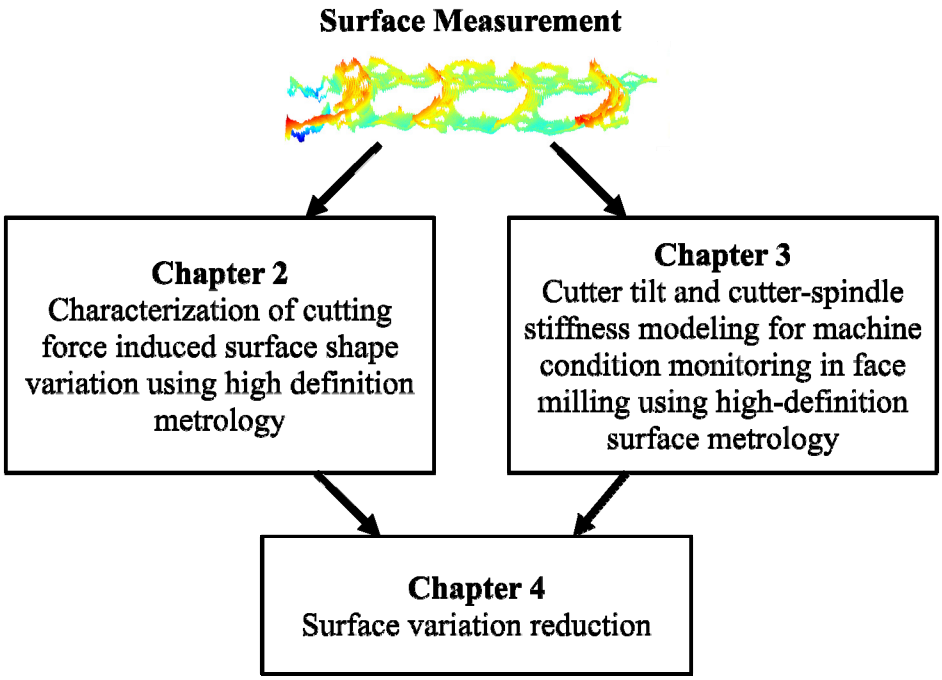

Figure 1-5 Research framework

CHAPTER 2

CHARACTERIZATION OF CUTTING FORCE INDUCED SURFACE SHAPE VARIATION IN FACE MILLING USING HIGH DEFINITION METROLOGY

High-definition metrology (HDM) systems with fine lateral resolution are capable of capturing the surface shape on a machined part that is beyond the capability of measurement systems employed in manufacturing plants today. Such surface shapes can precisely reflect the impact of cutting processes on surface quality. Understanding the cutting processes and the resultant surface shape is vital to high-precision machining process monitoring and control. This chapter presents modeling and experiments of a face milling process to extract surface patterns from measured HDM data and correlate these patterns with cutting force variation. A relationship is established between the instantaneous cutting forces and the observed dominant surface patterns along the feed and circumferential directions for face milling. Potential applications of this relationship in process monitoring, diagnosis, and control are also discussed for face milling. Finally a systematic methodology for characterizing cutting force induced surface variations for a generic machining process is presented by integrating cutting force modeling and HDM measurements.

2.1 Introduction

By using HDM data measured from machined surface, this chapter introduces a method of characterizing surface variation patterns. A model of cutting force is developed to correlate cutting force variation to surface variation patterns.

Machined surface patterns have been extensively studied in multiple scales. At fine scales (micron level), surface textures were correlated to a number of process conditions. Tool conditions were found to have a significant impact on surface texture, (Wilkison et al. [43] and Yi et al. [36]). Schmitz et al. [9] correlated tool runout, stability, and surface location errors to surface finish. Baek at al. [29] introduced a model to predict surface roughness that includes cutting conditions, edge profile, insert runout, and dynamic characteristics. Kline et al. [10] showed the effects of radial run-out and chip load on surface finish. Surface errors were also predicted along with cutting force considering system deflections (Sutherland et al. [48]). At coarse scales (from several millimeters to the form as defined in [35]), Takeuchi et al. [7] studied the effects of spindle tilt and thermal expansion on the surface form error. Camelio et al. [47] investigated the effect of fixturing and clamping on surface form error. Liao at al. [40] used FEM to model fixture-workpiece to study the influence of clamping preload and machining force on the machined surface quality. Gu et al. [39] used a finite element method called equivalent flexibility influence coefficient to predict the deformation of cutter-spindle and workpiece-fixture assembly. The relative position between cutter and workpiece can be predicted to estimate surface errors.

A number of models have been developed to estimate cutting forces in machining. Ruzhong et al. [25] characterized cutting force profile in face milling based on single tooth

cutting. Wang et al. [26] developed a convolution modeling method to predict the total cutting force in milling. Anderson et al. [22] studied how the cutting action of an insert is affected by neighboring inserts. Li et al. [24] predicted cutting forces of dynamic milling processes considering thermal effect. Wu [31] studied the dynamic cutting process by developing the transfer function between the vibration variables and the dynamic force components for a single degree-of-freedom machining system. Montgomery et al. [30] studied the effect of cutting dynamics on surface finish and established a relation between tooth passing frequency and a dominant frequency of tool-workpiece structure.

Due to a lack of metrology systems that are capable of measuring large surfaces with high resolution, the surface patterns such as those reflected by the HDM data in Figure 1-2 have not been studied in the previous research. Based on the LHI technology, this Chapter identifies surface distortion patterns and establishes the correlation with material removal rate. The shape patterns are extracted along the feed and circumferential directions of cutter movement. Along the circumferential direction, the cutting force variation due to different engagement of inserts with cutting is analyzed and correlated to surface patterns. Along the feed direction, the surface variation is compared with the cutting force changes due to the variations in material removal rate (MRR). The relationship between the MRR and surface height is quantified to characterize the shape patterns in this direction. Finally, we discuss the potential applications of the extracted surface patterns as well as new parameters/metrics that can be derived for process monitoring and product/process improvement.

The remainder of the chapter is organized as follows. We first describe the experiments and surface shape pattern extraction along the feed and circumferential directions, then conduct cutting force modeling along the two directions to interpret the shape patterns and discuss

applications of the extracted surface characteristics in process monitoring and improvement. Conclusions are given in the last section.

2.2 Experiments and extraction of shape patterns

Experiments are conducted to analyze the surface patterns along the feed and circumferential directions based on the HDM data, respectively. Spline filtering method is selected to extract the patterns.

2.2.1 Experiment setup

Face milling is used to cut the three solid blocks of Aluminum 2024-T351 with dimensions of 75x270x75 mm^3 (Figure 2-1). A large thickness value (75mm) is chosen to reduce the structural deformation. The depth of cut is 0.5mm; the feed rate is 0.5 mm/tooth; and the spindle speed is 1000 rev/min. The cutter has an effective diameter of 101.6 mm with five inserts. The face milling operation was implemented on a Cincinnati CNC machine (model HMC-400EP) and the machined surfaces were measured by a ShaPix^{TM} laser holographic interferometer.

In this experiment, three blocks with different geometry designs were prepared to investigate the impact of the MRR on surface profiles. The MRR determines the axial cutting force and is directly influenced by the geometry design such as size, shape, and spatial distribution of holes. Block 1 is solid (Figure 2-2a) which is used to study the variation of surface height along the circumferential direction. Block 2 (Figure 2-2b) has pockets whose curved edge has the same radius as that of the cutter. This surface design will cause drastic change of the MRR (volume of materials removed per revolution of the cutter) as the cutter moves along the feed direction. The Block 3 (Figure 2-2c) has holes with different diameters. This design can lead to a smoother change of MRR along the feed direction.

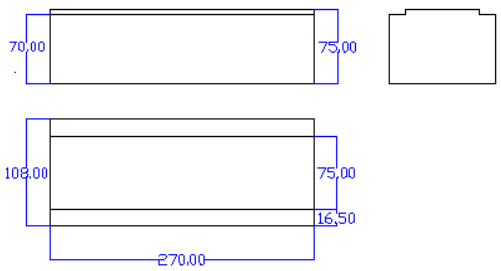

Figure 2-1 Dimensions of the aluminum blocks (mm)

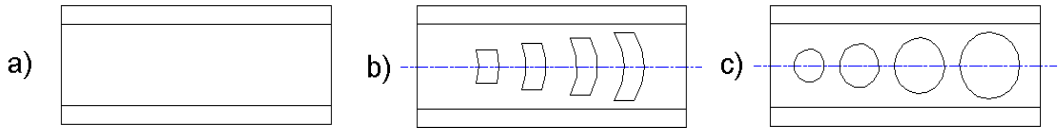

Figure 2-2 Geometries of the workpiece (a – Block 1, b – Block 2, c – Block 3)

2.2.2 Selection of filtering algorithm and image preprocessing

A machined surface has patterns with a wide range of spatial frequencies including roughness/ waviness (short wavelength) and form (large wavelength) [35]. Patterns at different frequencies are mainly extracted by using filtering methods [49] such as 2RC filter, Gaussian filter, Rk filter, spline filter, robust spline filter, Gaussian regression and robust Gaussian regression filters, and morphological filter. Spline filtering method is chosen for surface pattern extraction due to its efficiency in image processing with less boundary distortion and its robustness against outlier compared with other filtering methods.

To facilitate the filtering along the circumferential direction, the toolmark is first straightened by using a mapping function that transfer points on the insert trajectory curve to corresponding points on a straight line. Then the filtering is applied to the straightened profile. Figure 2-3a shows the toolmark produced by one insert on one revolution. The cutter path is

along the horizontal axis (X direction). The cutting point A rotates about the cutter center O_c which is moving along the cutter path. The front of the leading edge of the cutter is at D. Assume that the cutter moves along the X axis at the feed rate f (mm/s) and rotates at the speed of ω (ω = πS/30 (rad/s)), where S is the spindle speed (rev/min)). Assume that the cutting point start at a point A (t=0). At a given time *t*, the coordinates of the cutting point B are

$$\begin{aligned} X_B &= X_{Oc} + ft + R\sin\omega t \\ Y_B &= R\cos\omega t \end{aligned} \tag{2-1}$$

The time elapsed when the cutting point reaches the point B is $t_B = (a/\omega)\cos(Y_B/R)$. So, $XO_c = X_B - ft_B - R\sin\omega t_B$. When $\omega t = \pi/2$ (point D), one can have $t_D = \pi/(2\omega)$ and $OC_D = ft_D + R$. The projection plane can be any plane that perpendicular to the feed direction. It should goes through point D for convenience. The coordinates of the point (C) on the straightened path corresponding to the point B can be calculated by

$$X_C = X_{Oc} + O_C D = X_B + f(\frac{\pi}{2\omega} - t_B) + R(1-\sin\omega t_B) \tag{2-2}$$

$$Y_C = \begin{cases} \int_{t_P}^{t_D} \sqrt{\left(\frac{dx}{dt}\right)^2 + \left(\frac{dy}{dt}\right)^2}\, dt = \int_{t_P}^{t_D} \sqrt{\left(f + \omega R\cos\omega t\right)^2 + \left(R\sin\omega t\right)^2}\, dt, & 0 < \theta < \pi/2 \\ -\int_{t_D}^{t_P} \sqrt{\left(f + \omega R\cos\omega t\right)^2 + \left(R\sin\omega t\right)^2}\, dt, & \pi/2 < \theta < \pi \end{cases} \tag{2-3}$$

Using Eq. (2-2) and (2-3), the toolmark can be straightened by mapping all points along the toolmark onto a straight path as shown in Figure 2-3b-c.

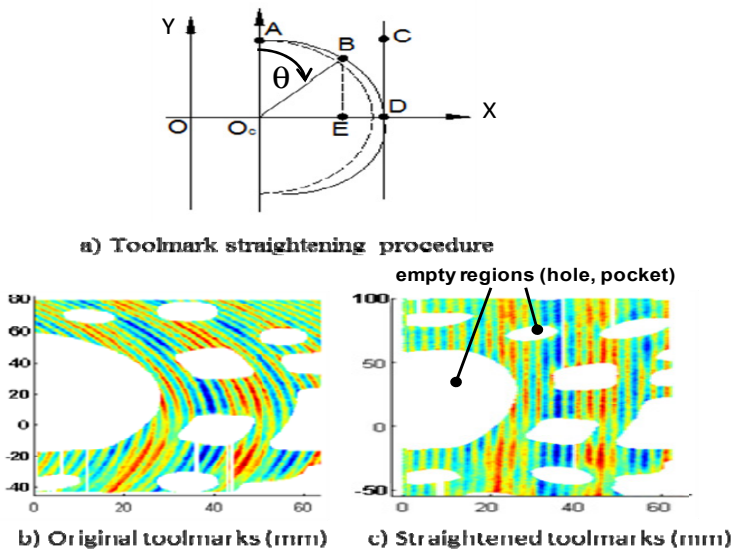

Figure 2-3 Toolmark straightening

2.2.3 Results

The measured surfaces of blocks 1, 2, and 3 are shown in Figure 2-4. The surface of Block 1 (Figure 2-4a-b) exhibits a high-low-high pattern in the circumferential direction whereas there is a lack of obvious pattern along the feed direction. The surface of Block 2 (Figure 2-4b) shows a pattern varying with the surface geometry design, i.e., the surface profile tends to be high where there more materials present without holes (higher MRR) and becomes low where the holes present (low MRR). The measured surface of Block 3 (Figure 2-4c) shares the similar pattern with Block 2. The only difference is that Block 2 shows a sharp profile jump near the edge of holes while the jump in Block 3 is smaller.

Surface patterns along the circumferential direction

The surface pattern along the circumferential direction can be shown in Figure 2-5. Figure 2-5a-e displays the insert engagement at different rotational angles of the cutter. Figure

2-5a shows the state when only insert 1 is engaged with the cutting. Then insert 5 begins to cut the part while insert 1 is still in cutting (Figure 2-5b). As the cutter rotates, both insert 5 and insert 1 are in cutting (Figure 2-5c). Figure 2-5d shows the state when insert 1 exits the part while insert 5 is engaged in cutting. The boundary between the zones with different grey scales in Figure 2-5f outlines the locations where the number of insert engaged in the cutting switches from one to two or from two to one.

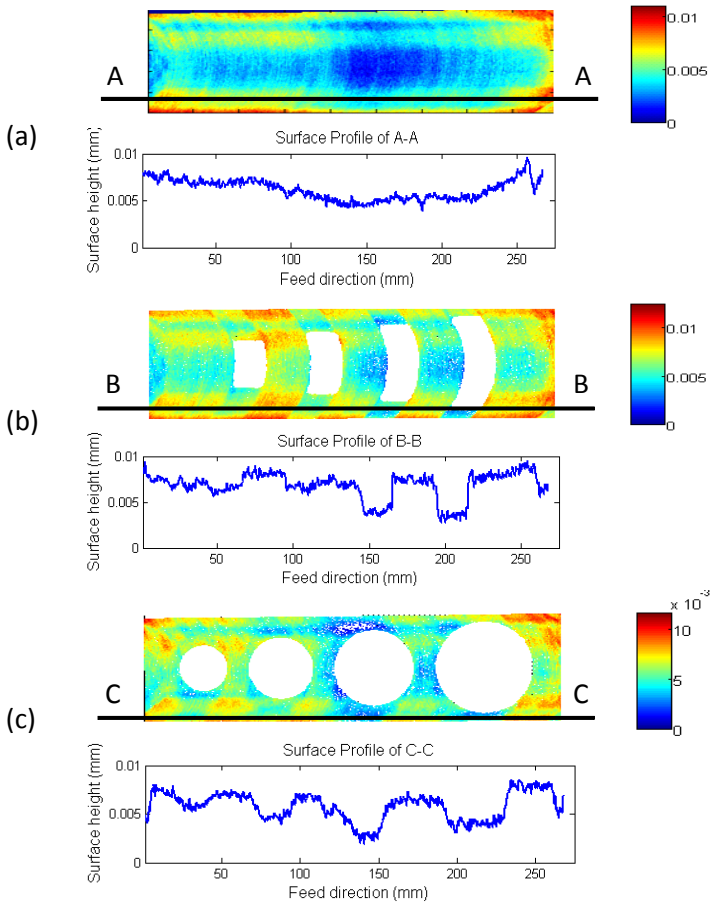

Figure 2-4 The measured surface and surface profile of block 1, 2, and 3 (a– Block 1, b– Block 2, c– Block 3)

The surface patterns in the circumferential direction can be extracted by suppressing the surface height variation in the feed direction caused by geometry complexity. A high-pass filter

is applied to the surface data along the circumferential direction to extract patterns at the wavelength less than the distance between inserts. The distance between inserts in the circumferential direction equals $2\pi R/N$ = 63.4 mm, where R is the radius of cutter and N is number of inserts. Thus, the cut-off wavelength of the high-pass filter is chosen to be 70 mm. In addition, a low-pass filter with a cut-off wavelength of 7 mm is used to remove fine-scale waviness pattern that is not the focus of this study. The result is shown in Figure 2-6.

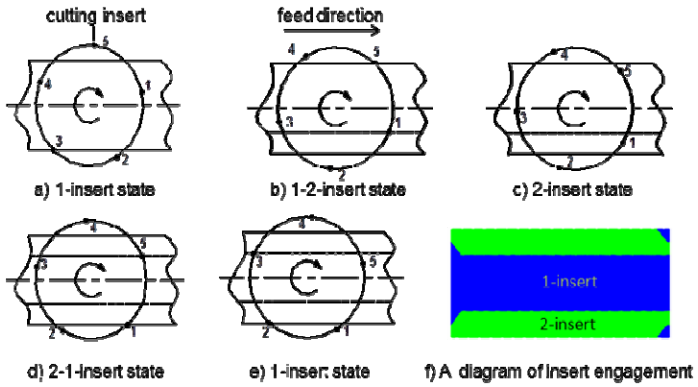

Figure 2-5 A description of cutting insert engagement

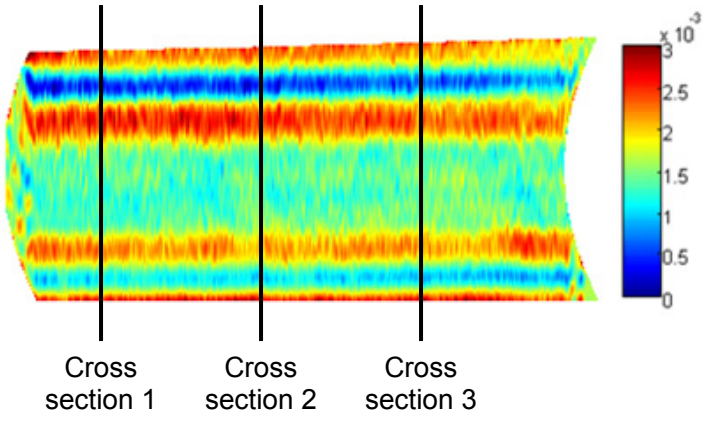

Figure 2-6 Extracted short wavelength patterns with toolmarks being straightened

The extracted pattern as shown in Fig. 2.6 shows strong similarity with the insert-engagement diagram (Figure 2-5) which describes areas of different cutting insert engagement on the surface. Three cross sections from Figure 2-6 are plotted in Figure 2-7 which shows that the area where the number of inserts engaged in the cutting switches between 1 and 2 has a jump in the profile. In addition, the distance between the peaks is close to that between the boundaries where the number of engaged inserts switches (approximately 42 mm). This phenomenon is caused by the cutting force variation along the circumferential direction and will be modeled in the next section. The same data processing procedure is applied into the surfaces of block 2 and 3 (Figure 2-8). The similar high-low patterns are observed.

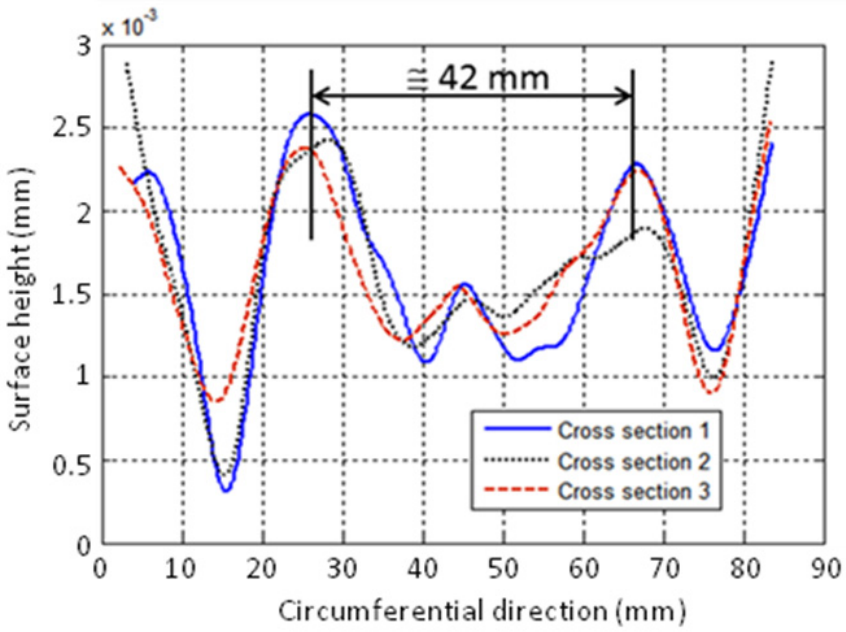

Figure 2-7 Profiles of the short wavelength pattern on Block 1

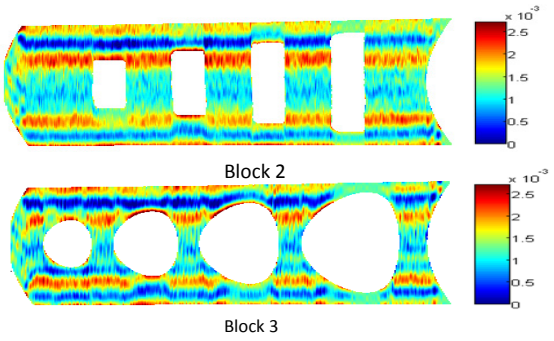

Figure 2-8 Short wavelength pattern on Block 2 and 3

Patterns along the feed direction

To extract the surface pattern along the feed direction, the surface height variation in the circumferential direction needs to be suppressed. A low-pass filter is applied at the cutoff wavelength of 75 mm and the surface profile along the circumferential direction is averaged. The resultant pattern after the filtering is shown in Figure 2-9. Figure 2-10 and Figure 2-11 are the scatter plots for the average height in the circumferential direction and normalized MRR. A positive correlation between the two variables is clearly presented.

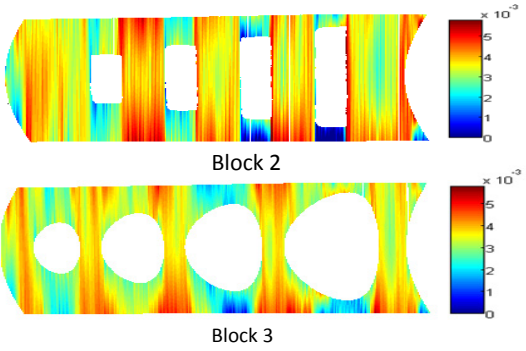

Figure 2-9 Extracted pattern along the feed direction (toolmarks straightened)

In summary, there exist relations between insert engagement, material removal rate (or surface geometry design) and surface profile. The next section will conduct cutting force modeling to explain the mechanism that generates these patterns.

2.3 Cutting force modeling and its correlation with shape variation

In this section, the axial cutting force is modeled and correlated to surface profile along the feed and circumferential directions, respectively. The modeling result is then validated based on the experimental data.

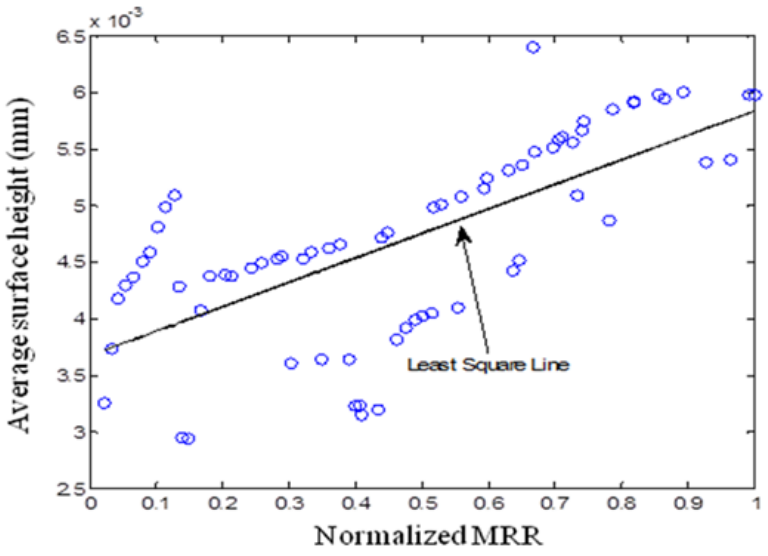

Figure 2-10 Surface height vs. MRR on Block 2

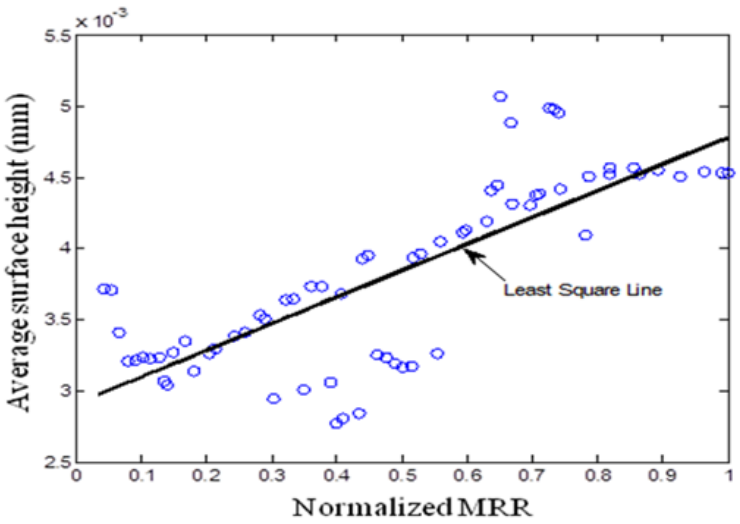

Figure 2-11 Surface height vs. MRR on Block 3

2.3.1 Model Development

Cutting force is one of the main factors that contribute to surface variations. As such, axial cutting force modeling is conducted to estimate the cutter-workpiece relative displacement.

Assume that the machine tool has a very small spindle tilt (less than 0.001 radian) and the depth of cut is considered a constant. It is also assumed that there is no relative displacement between inserts on the cutter.

Figure 2-12 shows the motion of the cutter relative to the workpiece as well as directions of the cutting forces exerted on each insert. The axial cutting force is the product of cross section area on the chip and the specific cutting pressure K_a which includes all the factors related to cutter geometry, cutter material, and workpiece material [23, 48]. Thus, the axial cutting force acting on insert i can be estimated by

$$F_{ai} = K_a f_t \sin(\theta_i(\phi))d \tag{2-4}$$

where $\theta_i(\phi)$ is the rotation angle of insert i when the cutter rotates at an angle ϕ; f_t is the feed rate per tooth; and d is the depth of cut.

With N cutting inserts, the total amount of axial cutting force applied on the cutter at certain insert angle θ is

$$\begin{aligned} F_a &= \sum_{i=1}^{N} \delta(\theta_i(\phi)) F_a(i,\phi) = K_a d \sum_{i=1}^{N} \delta(\theta_i(\phi)) C_i(\theta_i(\phi)) \\ &= K_a d f_t \sum_{i=1}^{N} \delta(\theta_i(\phi)) \sin\theta_i(\phi) \end{aligned} \tag{2-5}$$

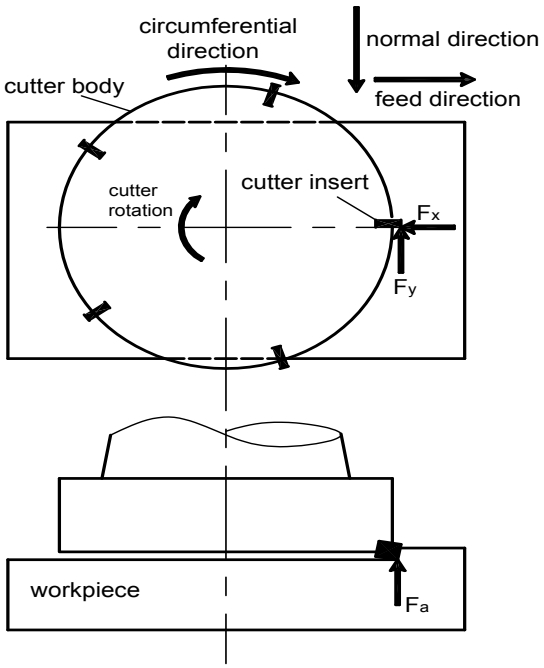

Figure 2-12 The Cutting force diagram for the cutter-workpiece system

where $\delta(\theta_i)$ is an indicator function that implies whether or not the insert i is engaged in a cutting process, i.e. [48],

$$\delta(\theta_i(\phi)) = \begin{cases} 1 \quad if \quad \xi_{01} \le \theta_i(\phi) \le \xi_{11} \quad or \\ \qquad\qquad ... \qquad\qquad or \\ \qquad\quad \xi_{0n} \le \theta_i(\phi) \le \xi_{1n} \quad or \\ 0 \qquad\quad otherwise \end{cases} \tag{2-6}$$

where $\xi_{11, \ \ldots, \ } \xi_{0n}$ are the angles that specify the boundaries as well as slots on the workpiece as shown in (Figure 2-13). The first subscript in ξ_{ij} represents whether the insert is entering or exiting a part, i.e., i=1 for the entry and i=0 for the exit. The second subscript j stands for the jth material region in the circumferential direction.

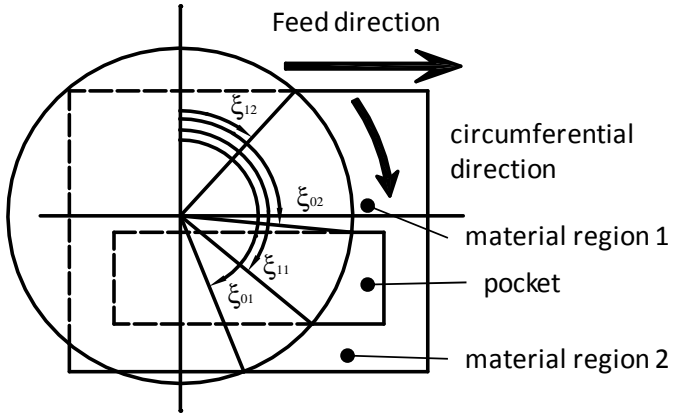

Figure 2-13 Cutter rotational angles

The variation of surface height along the cutting path can be studied by averaging the cutter-workpiece displacement over each cutting revolution. The cutter-workpiece displacement at a given rotational angle of cutter ϕ can first be represented by

$$\begin{aligned} &\Delta h = K_d F_a \\ &= K_d \sum_{i=1}^{N} \delta(\theta_i(\phi)) F_a(i,\phi) = K_d K_a d \sum_{i=1}^{N} \delta(\theta_i(\phi)) C_i(\theta_i(\phi)) \\ &= K_d K_a d f_t \sum_{i=1}^{N} \delta(\theta_i(\phi)) \sin\theta_i(\phi) = K_1 \sum_{i=1}^{N} \delta(\theta_i(\phi)) \sin\theta_i(\phi) \end{aligned} \tag{2-7}$$

where K_d is the stiffness of cutter-workpiece and $K_1 = K_d K_a df_t$. All the inserts that are engaged in cutting are assumed to create the same displacement Δh. Then the average cutter-workpiece displacement of a single insert over one revolution will be the integration of Δh over the effective cutting length per revolution, i.e.,

$$\overline{\Delta h} = \frac{1}{2\pi R} K_1 \int_0^{\pi} ds = \frac{1}{2\pi} K_1 \int_0^{\pi} \sum_{i=1}^{N} \delta(\theta_i(\phi)) \sin\theta_i(\phi) d\phi \tag{2-8}$$

Denote K2 = K1/(2πR) = KdKadft/(2πR) and let

$$L = \int_0^{\pi} \sum_{i=1}^{N} \delta(\theta_i(\phi)) \sin\theta_i(\phi) d\phi$$

which can be estimated by

$$L = \sum_{i=0}^{N-1} \sum_{j=1}^{n} \int_{\xi_{1j}}^{\xi_{0j}} \delta(\theta(\phi) - \frac{2\pi}{N} i) \sin(\theta(\phi) - \frac{2\pi}{N} i) d\phi \tag{2-9}$$

Thus, $\overline{\Delta h} = K_2 L$. Equation (2-8) implies that the average cutter-workpiece displacement over one revolution is proportional to the sum of lengths of insert trajectory projected onto the direction perpendicular to the feed direction. For example, the average insert-workpiece displacement for a part as shown in Figure 2-14 is

$$\overline{\Delta h} = K_2 (l_{11} + l_{21} + l_{22} + l_{15}) \tag{2-10}$$

where l_{ij} is the projection of the trajectory of insert i on material regions j in the circumferential direction.

In addition, the parameter K_2 derived from Eq. (2-8) is directly related to the depth of cut (d), feed rate (f_t), radius of cutter (R), stiffness of cutter-spindle (K_d) and cutting pressure (K_a).

Therefore, K_2 has the potential as a parameter for process monitoring and will be discussed in the next section.

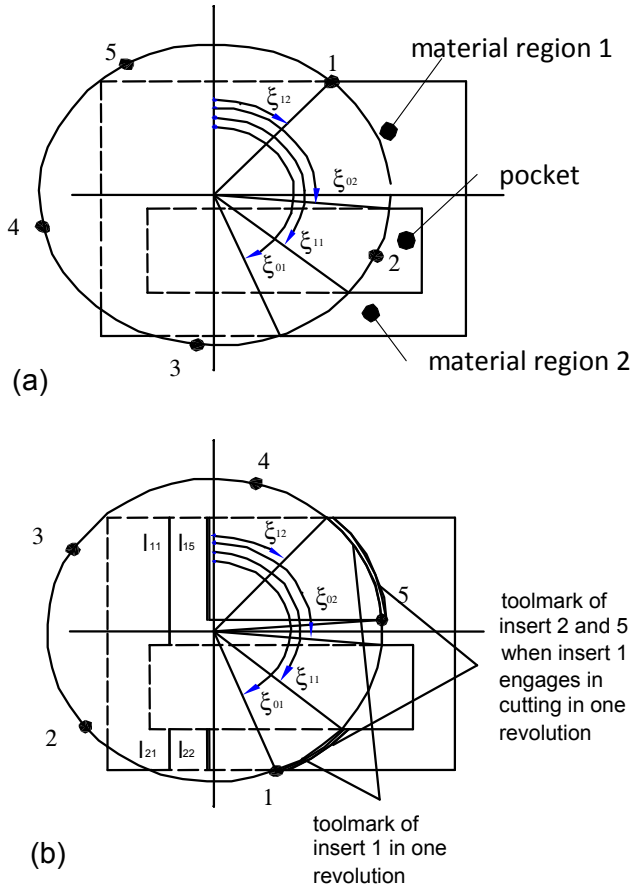

Figure 2-14 An example of the insert path (a – insert 1 enters cutting, b – insert 1 exists cutting)

The total length of the insert projection L can be simply approximated by the arc length of the toolmark. When the number of insert is more than ten, the projection length L is proportional to the arc length of the toolmark, as shown in Figure 2-15, i.e., $L=K_3L_{arc}$, where L_{arc} is the length of toolmark and K_3 can be estimated by linear regression based on the data in Figure 2-15. Table I shows a number of simulated values of K_3 given different insert numbers for Block

3. In practice, a face mill cutter may have more than 20 inserts installed and therefore this approximation is mostly applicable.

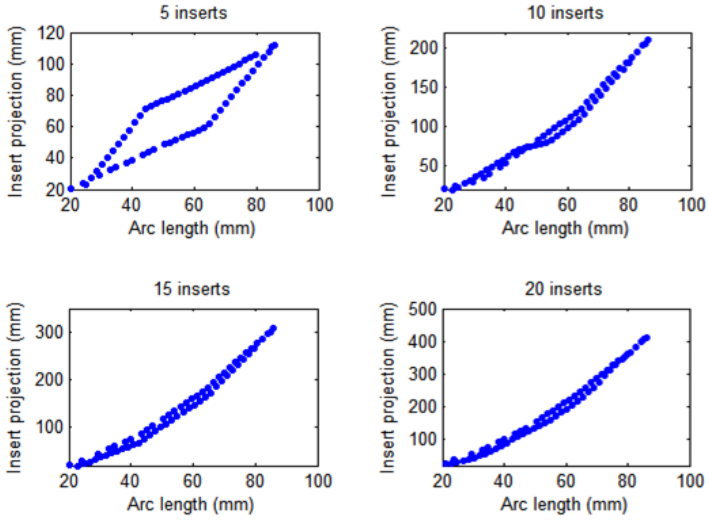

Figure 2-15 Relationship between the insert projection length (l) and toolmark length for different number of insert (Block 3)

Table 2-1 K_3 for different number of inserts N (Block 3)

N	10	11	12	13	14	15	16	17
K_3	3.051	3.472	3.821	4.106	4.431	4.784	5.139	5.439
N	18	19	20	21	22	23	24	25
K_3	5.745	6.069	6.410	6.745	7.040	7.360	7.700	8.016

Using the length of toolmark L_{arc}, the correlation between the MRR and surface profile can be represented in a linear form. In fact, by the definition of MRR, we have

$$MRR = L_{arc} df \tag{2-11}$$

So,

$$\overline{\Delta h} = K_2 L = K_2 K_3 L_{arc} = K_d K_a K_3 MRR / 2\pi RN = K_4 MRR \qquad (2\text{-}12)$$

where $K_4 = K_d K_a K_3 / 2\pi RN.$

2.3.2 Model Validation

Figure 2-16 compares the predicted average cutter-workpiece displacement with the measured average surface profile of Block 2 and Block 3, respectively. The predicted surface pattern was linearly scaled between 0-1 using the maximum surface variation range. It can be seen that the variation patterns of the measured surface height (Figure 2-16a and Figure 2-16d) and the surface pattern prediction based on cutting forces (Figure 2-16b and Figure 2-16e) are positively correlated (Figure 2-16c and Figure 2-16f).

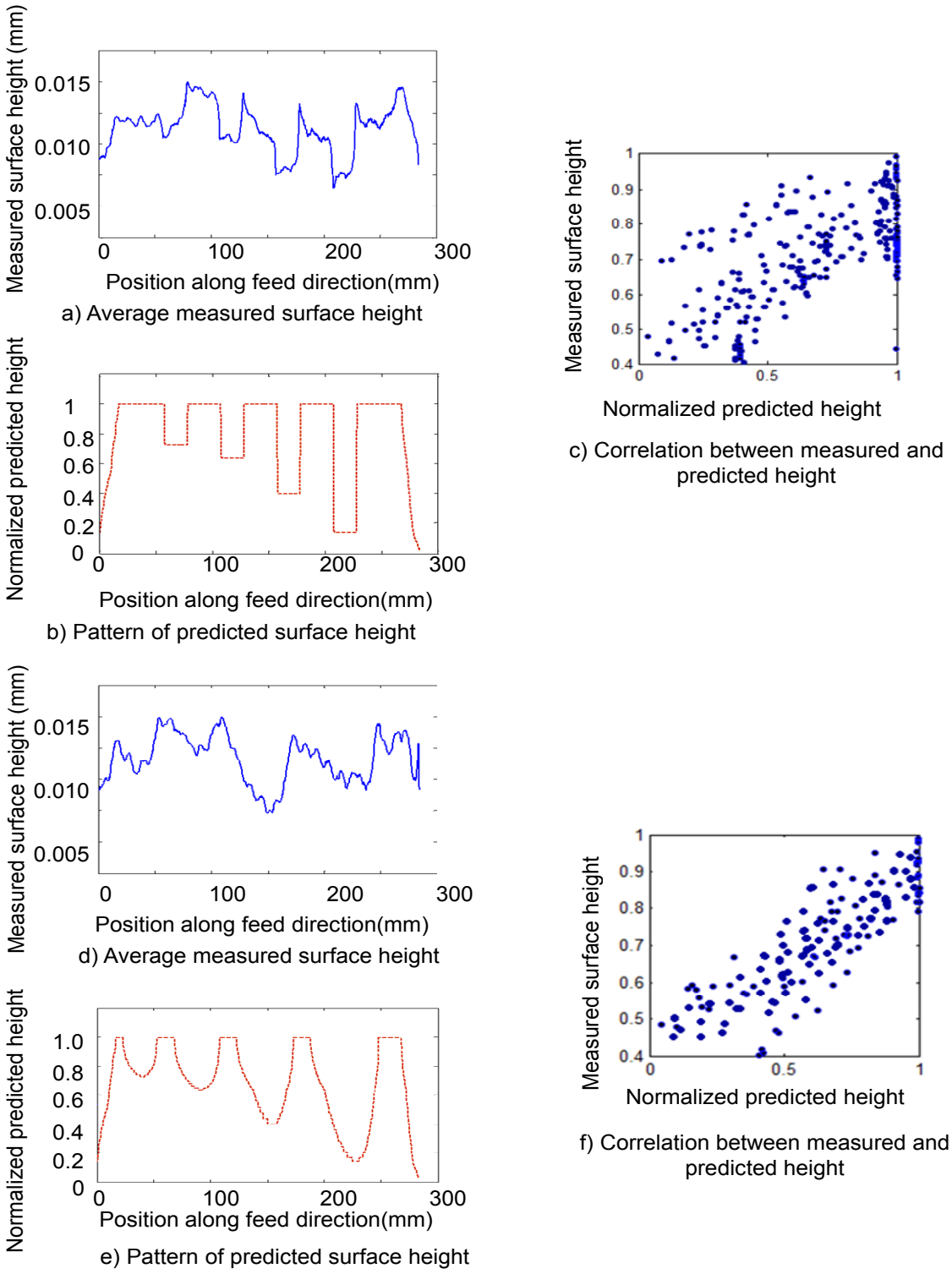

Figure 2-16 Comparisons of the predicted and measured average surface height along the feed direction on blocks 2 and 3

Figure 2-17 shows the predicted axial force based on Eq. (2-5) on Block 1. It shows an agreement between the predicted force and extracted surface patterns in the circumferential direction (Figure 2-6). The comparison of predicted force and extracted surface profile along the circumferential direction is given in Figure 2-18. The abrupt changes in cutting force also match the jump locations of surface profile.

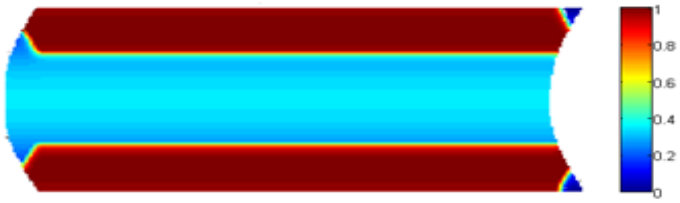

Figure 2-17 Normalized predicted axial cutting force distribution on block 3

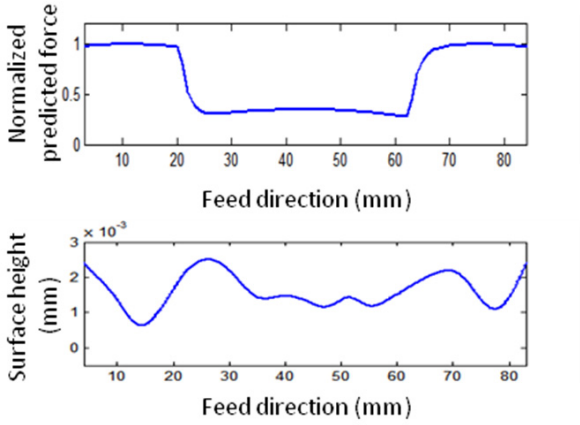

Figure 2-18 A comparison between the cutting force and surface profile along the circumferential direction

2.4 Discussions

Figure 2-19 shows the relationship between the MRR and surface height for a deck face of an engine head. The cutter has 24 inserts with an effective radius of 117.7 mm. The engine

head is mounted on a cast iron adapter plate during milling. The cutting process is more robust to variation sources such as vibration or fixture-induced part deformation. So, the MRR and surface height are strongly correlated.

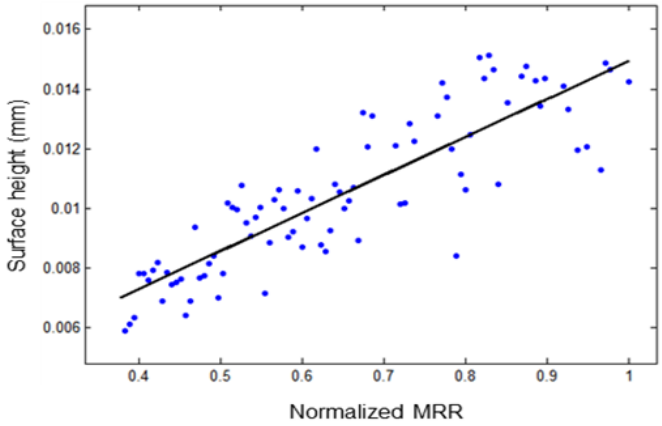

Figure 2-19 A scatter plot of the surface height vs. MRR on for an engine head deck face

Along the circumferential direction, the agreement between the extracted surface pattern along the circumferential direction (Figure 2-6) and the cutting force distribution diagram (Figure 2-17) implies that the pattern can be partially explained by the effect of cutting force changes due to the insert engagement. The discrepancy could be explained by higher order effect of dynamic cutter-workpiece system in the future study, such as using a damping and spring model.

2.5 Summary and Potential Applications

The methodology of characterizing cutting force induced surface variations is summarized in Figure 2-20. The procedure begins with cutting force modeling that captures cutting force spatial distribution over the surface. Meanwhile, HDM measurement is performed on the machined surface. The surface features are extracted by filtering the HDM data along the

direction of interest as determined by comparing cutting force prediction with measured surface patterns. Process parameters that impact the surface features are identified from the model. The obtained parameters provide means of process monitoring and control of surface variations.

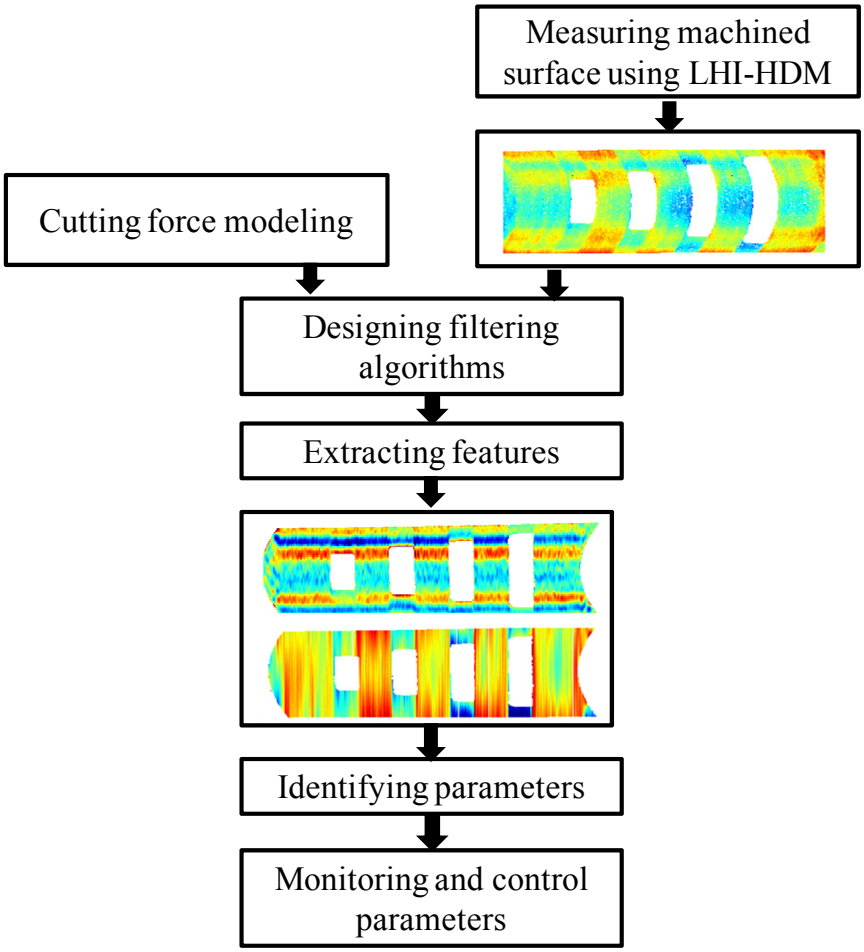

Figure 2-20 Methodology review

We now discuss the potential applications of the extracted surface patterns due to cutting force dynamics in product design, machining process monitoring, and improvement.

Part design for machining. The relationship between the MRR and surface height variation can be utilized in part design. The workpiece should be designed in a way to avoid high MRR variation along the feed direction. Holes, slots, or pockets should be distributed equally

over the surface, as shown in Figure 2-21. Design 1 has two zones with high MRR, generating two jumps in these areas. If functional performances are not affected, the design can be improved by moving two small holes to the high-MRR area (Design 2). But the jump on the right end still exists. Design 3 has the smallest MRR variation among the three designs.

Machining improvement. Based on the linear correlation between the MRR and surface height, one can increase and reduce the feed rate to compensate for the MRR variation along the feed direction induced by surface geometry. The resultant surface profile generated by the varying-feed method as outlined in Figure 2-22 is expected to exhibit less variation.

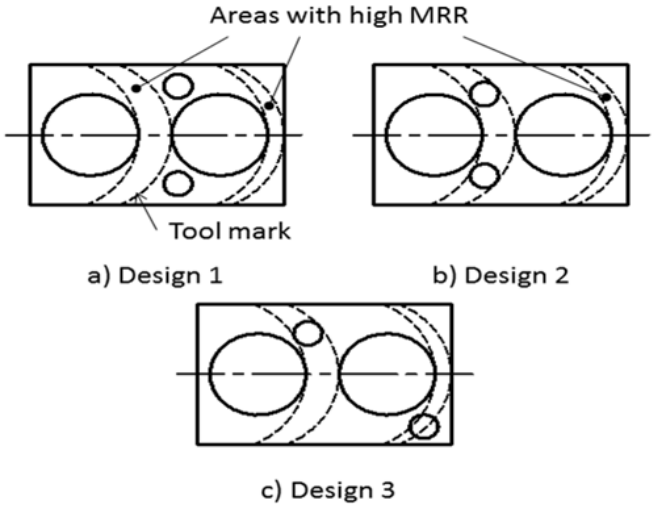

Figure 2-21 Part design improvement for reducing the MRR variation

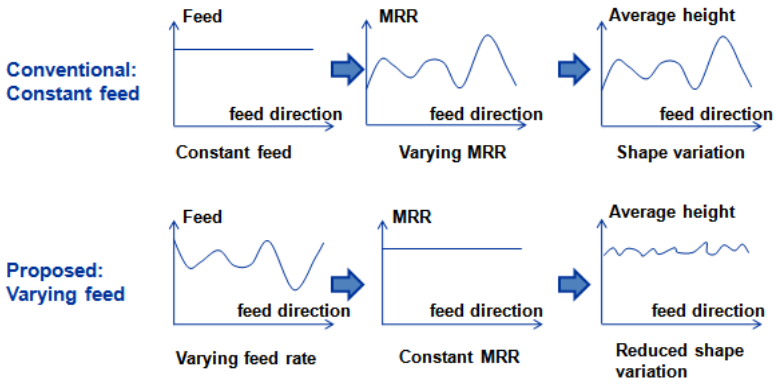

Figure 2-22 Surface variation reduction using a varying feed method

Another application of the MRR vs. height relationship can be in understanding and reducing the singularities on machined surfaces. Figure 2-23a shows a jump on the wing section of an engine head. Such a surface singularity is critical for the assembly between the engine head, gasket, and engine block. It is generated when the middle section of the cutter begins to hit the firing deck, thus resulting in a high MRR change along the feed direction (Figure 2-23b). The MRR variation in this case could increase the flatness up to 40 microns. Using the varying-feed rate method could be effective; however, it may potentially lead to an extremely high feed rate that is able to compensate for the loss of MRR on the wing section. An alternative method can be to use a non-straight entry cutter path that mitigates the MRR variation on the wing section to reduce the jump. The detailed algorithm is being developed in another work of our related research.

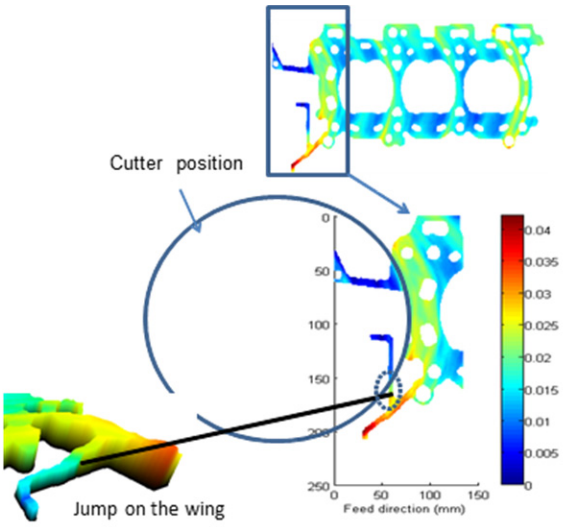

(a)

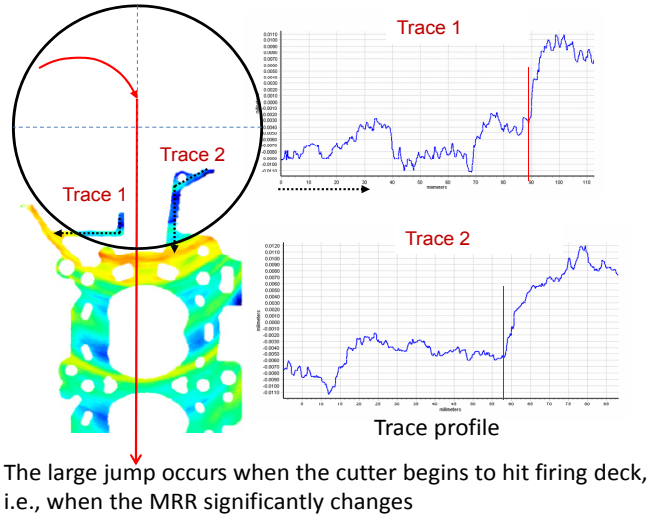

(b)

Figure 2-23 An engine head and surface error caused by the MRR variation

Tool life monitoring. The relationship between the MRR and surface height is also influenced by the remaining tool life. Figure 2-24 shows that the coefficient K_4 in Eq. (2-12) is negatively related to the remaining tool life. Therefore, the average value of K_4 (K_2 for cutter

with few inserts) contains tooling information and could be used as a parameter for monitoring tooling conditions (by performing a t-test of null hypothesis that the values of K4 when the remaining tool life is 43% and 75% (Fig. 2-24), the result indicates a rejection of the null hypothesis with p-value equal to 0.0625). Another application of such a relation can be in tool replacement planning. In a CNC face milling process of automotive engine heads, engineers usually replace the face mill cutter when the jump as shown in Figure 2-23 exceeds certain value of the surface span flatness specification. The new cutter is effective in bringing the jump down below the specification limit. The rationale behind this practice is that the jump on the wing section will be more significant for a worn tool since the impact (K_4) of the surface geometry (or MRR) on the surface flatness increases as the tool wears. As the tool is replaced, though the jump still exists, it is suppressed (below the specification limit) due to a reduced K_4. It can be expected that the tool life change interval could be potentially increased by appropriately selecting cutter path or feed rate.

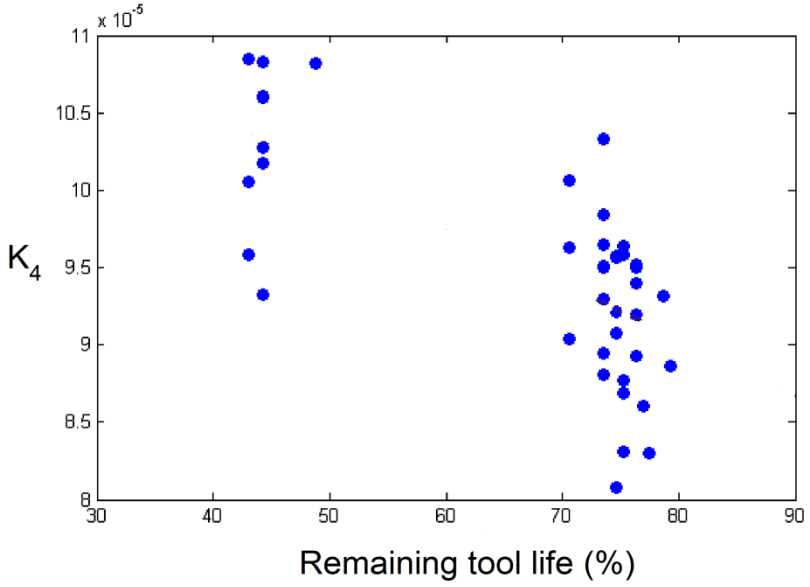

Figure 2-24 K_4 vs. remaining tool life

Clamping condition monitoring. The surface pattern along the circumferential direction could be useful for detecting faulty process conditions such as a clamping error. Block 1 was milled under the faulty clamping by which the part datum surface is not fully supported by the fixture. The same procedure for Figure 2-6 was applied to extract the surface patterns along the circumferential direction and the result is shown in Figure 2-25. It can be seen that the pattern is very different and the distance between peaks (≅42 mm) is not relatively a constant. The irregularity of the extracted patterns is related to the sensitivity of the dynamic response of cutter-workpiece system.

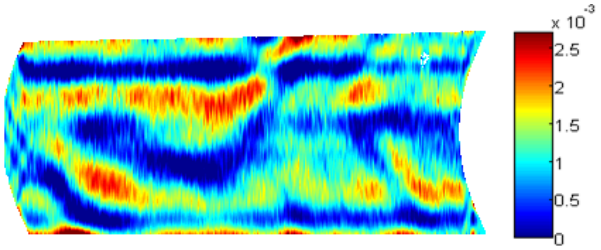

Figure 2-25 Surface pattern induced by insert engagement variation under a faulty clamping condition (Block 1)

2.6 Conclusions

This study identified new surface variation patterns measured by the HDM along the circumferential and feed directions on a face milled surface. Cutting force modeling is conducted to interpret these surface patterns. Given the cutting conditions and surface geometry, a cutting force model is established to estimate the relative displacement of cutter-workpiece. The following conclusions are drawn from this study:

- In the circumferential direction, it is found that surface profiles are correlated to the axial cutting force. At the boundary where the number of inserts engaged in cutting changes, cutting force changes abruptly and results in jumps in the surface height profile. This pattern is found to be sensitive to dynamic change of cutter-workpiece such as clamping errors so that it can be used to detect changes in the cutting conditions.
- In the feed direction, it is found that surface variations are attributed to cutting force changes caused by the surface geometry induced MRR variations.

These findings will lead to important insights on surface design, process monitoring and improvement by maintaining a constant rate of material removal.

CHAPTER 3

MODELING CUTTER TILT AND CUTTER-SPINDLE STIFFNESS FOR MACHINE CONDITION MONITORING IN FACE MILLING USING HIGH-DEFINITION SURFACE METROLOGY

In face milling, the spindle is intentionally tilted to avoid backcutting. The real time cutter tilt during machining is a combined effect of the intentional tilt and cutter-spindle deflection, which varies with cutting load during machining. An accurate estimation of the cutter tilt is critical to surface quality control and machine health monitoring. However, due to the small magnitude, the spindle tilt and deflection are difficult to measure in real time. Conventionally, the cutter tilt can be obtained through in-line sensors mounted on the machine tool but this in-line measurement is greatly influenced by dynamic machining conditions such as vibration. This chapter proposes a method to monitor the spindle set up tilt and deflection using surface data measured by high-definition metrology (HDM). Two parameters are developed to characterize the cutter tilt, i.e., cutter tilt at idle state (initial cutter tilt) for spindle set up and cutter-spindle stiffness for the cutter-spindle deflection. Cutting force modeling is conducted to estimate these two parameters in conjunction with statistical procedures that fit the model to HDM surface data. The estimated cutter-spindle stiffness variation is also correlated to machine conditions such as a loose or worn bearing for process diagnosis.

The method is demonstrated via experimental data and a machining process of automotive engine heads.

3.1 Introduction

In a face milling operation, a cutter can be tilted as a result of spindle set up and cutter-spindle system deflection. To avoid backcut, the spindle is set up with a small amount of tilt (Figure 3-1a) at idle state when the cutter is not engaged in machining, i.e., initial cutter tilt $\beta 0$. In addition, the cutter tilt is also affected by the cutter-spindle system deflection caused by cutting forces (Figure 3-1b). The spindle-cutter deflection $\Delta\beta$ could either increase or decrease the cutter tilt. The resultant cutter tilt β as a combination of the initial cutter tilt and cutter-spindle deflection ($\beta = \beta_0 + \Delta\beta$) instantly varies with cutting load along the cutter path. The tilt angle can be measured by the angle between a tilting plane and workpiece surface, as illustrated in Figure 3-1b.

An instant cutter tilt could impact surface shape. An excessive instant tilt angle will create a surface with poor flatness which affects product performance such as sealing and distortion of assembly components. A small tilt angle can cause backcutting marks (Figure 3-1c) on the machined surface that subsequently reduce surface quality and tool life. Therefore, a method of estimating and controlling the instant cutter tilt is critical for surface quality control.

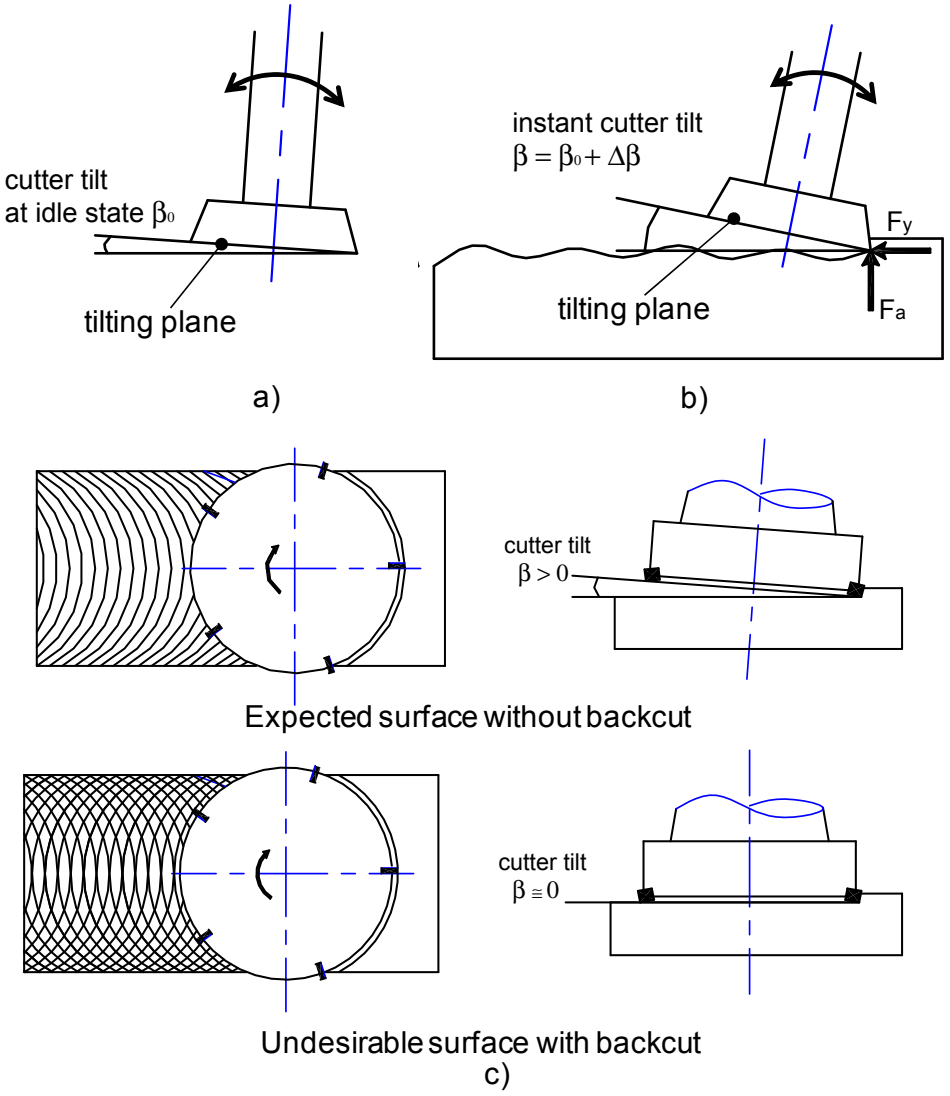

Figure 3-1 Cutter tilt during machining and its impact on surface quality

The instant cutter tilt reflects cutter and spindle conditions and provides potential variables for process monitoring. Abnormal variations in spindle set up can be detected by monitoring the initial cutter tilt. In addition, the cutter-spindle deflection reflects cutter-spindle stiffness under cutting force moment and monitoring the stiffness can help determine cutter-spindle health conditions. Figure 3-2 illustrates the components in cutter-spindle assembly that contribute to the spindle deflection (such as

tool holder, spindle, and bearing of ball screws). The stiffness of the system is sensitive to the condition changes in assembly components, e.g., a bearing being loose or worn on the spindle assembly and ball screw. The stiffness variation can cause the deflection of cutter-spindle which changes the instant cutter tilt, thus affecting the surface shape.

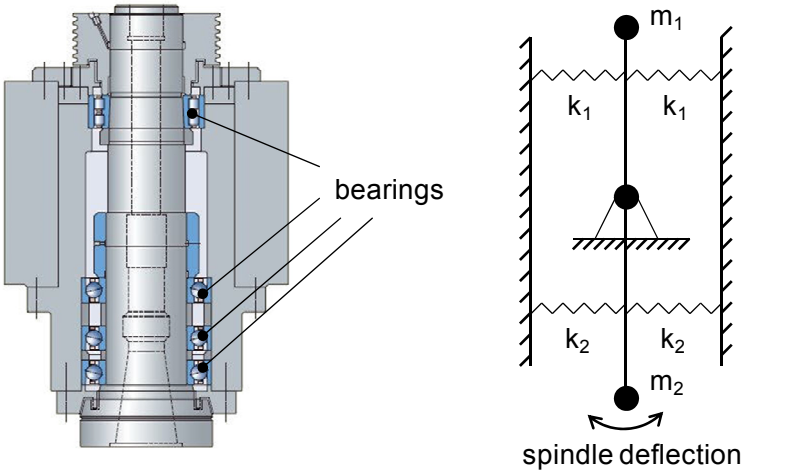

a) A design of spindle assembly

b) A demonstration of spindle deflection model

Figure 3-2 An example of cutter-spindle assembly: a) A design of spindle assembly (www.mycncuk.com), b) A demonstration of spindle deflection model

However, estimating and monitoring the instant cutter tilt are challenging because: (1) The cutter-spindle deflection varies with cutting load, making the instant cutter tilt vary along each cutting pass and differ among different part types (Figure 3-3); (2) The cutter tilt is often very small (about 0.001 rad) and is very difficult to measure; (3) The in-line measurement of tilt is subject to various noises during the machining and normal production needs to be stopped to perform these in-line measurements.

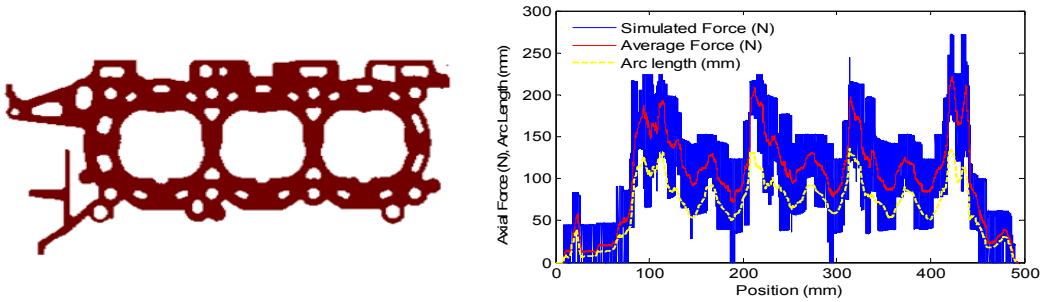

a) Workpiece geometry b) Simulated cutting force

Figure 3-3 A workpiece with varying geometry a) Workpiece geometry b) Simulated cutting force [50]

One alternative method of estimating the initial cutter tilt and cutter-spindle deflection is to calculate the tilting angle (β) of a plane formed by cutting inserts (Figure 3-1) on the machined surface. However, the success of this approach requires that fine surface features (such as tool marks) be captured by high-density spatial data so that the tilting plane and its tilt angle can be identified. The new type of high-definition metrology system based on laser holographic interferometry is adopted which can provide high-density data to characterize surface shape in detail (Figure 3-4) with high measurement speed. This metrology system presents an opportunity to develop an efficient method of monitoring machine conditions based on the routine surface quality inspection.

The spindle tilt can be roughly estimated by the Kirchner-Schulz formula [51] using the cross section of surface profile normal to the feed direction, as shown in Figure 3-5. However, the formula does not differentiate the difference between the initial cutter tilt and instant cutter tilt for monitoring and diagnosis, resulting in low estimation precision. It also requires the machined surface to be continuous (i.e., without holes or pockets).

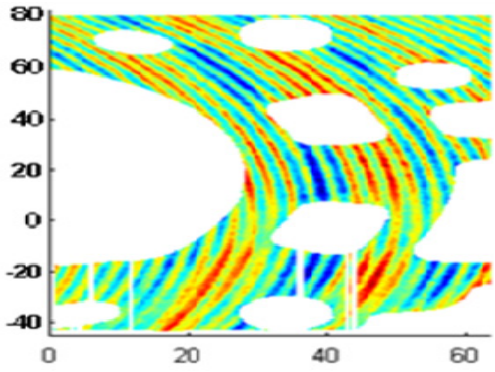

Figure 3-4 Machined surface captured by LHI with clear toolmarks [52]

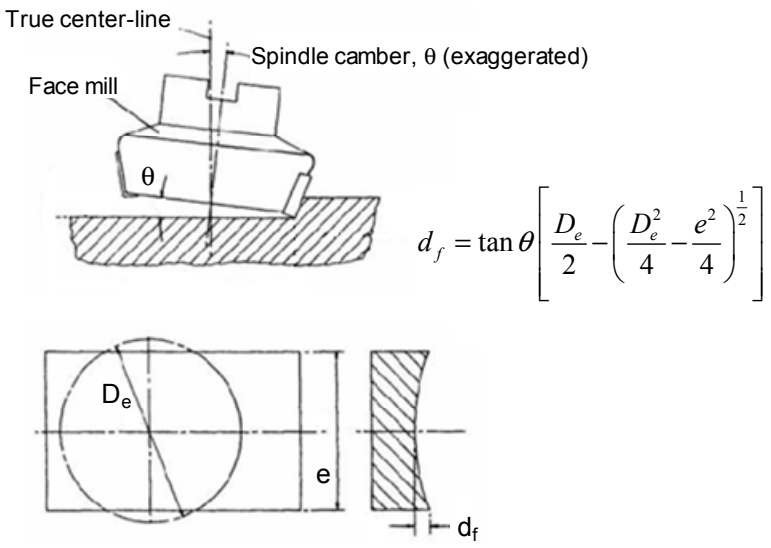

Figure 3-5 Estimation of spindle tilt angle using Kirchner-Schulz formula [51]

A number of models to estimate cutting forces and resultant surface shapes in machining were developed assuming a constant spindle tilt angle. For example, Gu et al. predicted the machined surface [39], while Andersson et al. [22] and Li et al. [24] and Fu et al. [23] studied cutting force in milling. Hun-Keun et al. [41] used sensor to detect spindle motion to predict roughness of machined surface. Sutherland et al. [48] predicted cutting force considering system deflections. Takeuchi et al. [7] studied the effects of spindle tilt and thermal expansion on the surface form error.

Extensive research has been conducted on machine health monitoring using in-line sensors. Takata et al. [53] introduced a method of monitoring tool breakage by means of monitoring fluctuations in spindle rotational speed. Erturk et al. [6] used an analytical model to select monitoring parameters in spindle-holder-tool assembly to maximize chatter stability. The spindle speed was monitored and controlled to stabilize chatter (Smith et al. [32-33]) and compensate for radial run-out of cutter (Sridhar et al. [54]). Research was also conducted to utilize surface data for process monitoring. Yi et al. [36] used surface data measured by the LHI to predict tool wear. Others [9-10, 29, 43] have used surface data measured by profilometers to predict cutter conditions. However, there is a lack of methods using the surface data to capture the instant cutter tilt and thereby monitor machining conditions. As indicated above, the HDM data can reveal surface rotational characteristics that are attributed to the instant cutter tilt; but no studies have explored the opportunities presented by surface HDM to estimate the cutter tilt and cutter-spindle stiffness.

To fill the research gap, this paper proposes an approach for spindle condition monitoring based on HDM data. A cutter-spindle deflection model is first developed to capture the relationship between the instant cutter tilt and the moment of cutting forces. The instant cutter tilt is then estimated from HDM surface data and combined with the established model to extract the cutter tilt at idle state and cutter-spindle system stiffness. The estimated parameters will be used to monitor the cutter-spindle conditions.

The remainder of the chapter is organized as follows. Section 3.2 conducts modeling of cutter-spindle deflection. Section 3.3 discusses statistical algorithm of calculating cutter tilt and stiffness from HDM data. The application of the model in

assisting machine setup and monitoring will be discussed in Section 3.4. Conclusions are given in Section 5.5.

3.2 Cutter-spindle deflection modeling

This section develops a cutter-spindle deflection model that relates the cutter tilt to the moment of cutting force along spindle axial and feed directions. The model also takes into account the effect of tool wear that impacts prediction precision. The cutter-spindle deflection model will be developed based on an assumption that the relationship between instant cutter tilt and moment of cutting load is linear. Thus, the moment induced cutter-spindle deflection ($\Delta\beta$) is proportional to the moment of cutting force.

Figure 3-6 shows the diagram of cutting force for a cutter-spindle system with an initial tilt. Cutting forces F_{zi}, F_{yi} applied on insert i cause the cutter-spindle to deflect in opposite directions. With the assumption that the cutting force in each direction equals the product of cross area of chip at current position of insert and cutting pressure in that direction [23], the axial cutting force on insert i can be estimated by

$$F_{zi} = P_z C_i(\theta_i(\phi))d \tag{3-1}$$

where P_z is cutting pressure on insert in axial direction, d is depth of cut and $C_i(\theta_i(\phi))$ is chip load of insert i at rotational angle θ_i and the cutter is at rotational angle of ϕ.

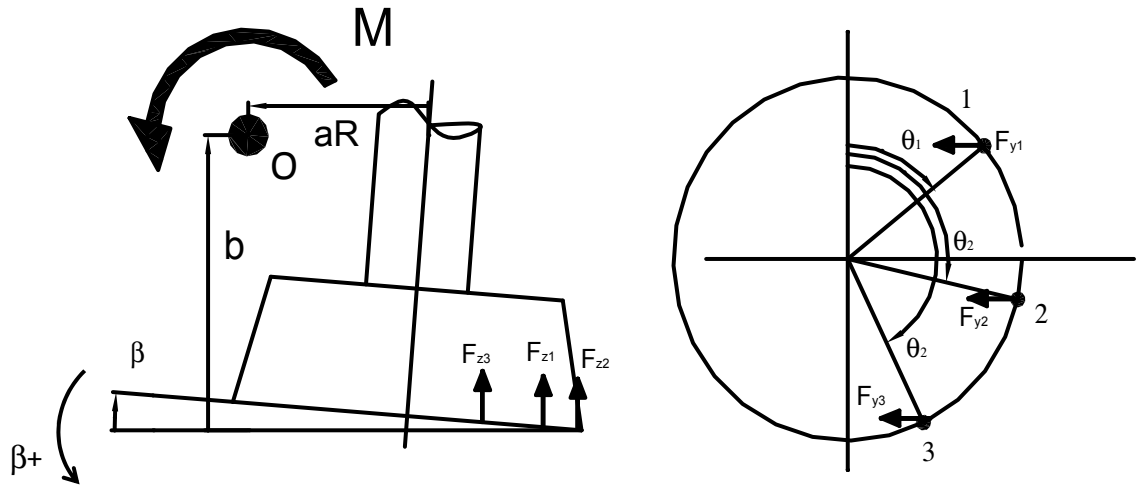

Figure 3-6 Cutting forces in axial and feed directions

The total axial cutting force is

$$\begin{aligned} F_z &= \sum_{i=1}^{N} \delta(\theta_i(\phi)) F_{zi}(\phi) \\ &= P_z d \sum_{i=1}^{N} \delta(\theta_i(\phi)) C_i(\theta_i(\phi)) \\ &= P_z d . f_t \sum_{i=1}^{N} \delta(\theta_i(\phi)) \sin\theta_i(\phi) \end{aligned} \tag{3-2}$$

where N is total number of inserts, $\delta(\theta_i)$ is an indicator function that implies whether or not the insert i is engaged in a cutting process.

$$\delta(\theta_i(\phi)) = \begin{cases} 1 \quad if \quad \xi_{01} \le \theta_i(\phi) \le \xi_{11} \quad or \\ \qquad\qquad ... \qquad\qquad or \\ \qquad\quad \xi_{0n} \le \theta_i(\phi) \le \xi_{1n} \quad or \\ 0 \qquad\quad otherwise \end{cases} \tag{3-3}$$

where ξ_{11}, … , ξ_{0n} are the angles indicating boundaries as shown in (Figure 3-7). The first subscript in ξij represents whether the insert is entering or exiting a part: i=1 for the entry and i=0 for the exit. The second subscript j stands for the *jth* material region in the circumferential direction.

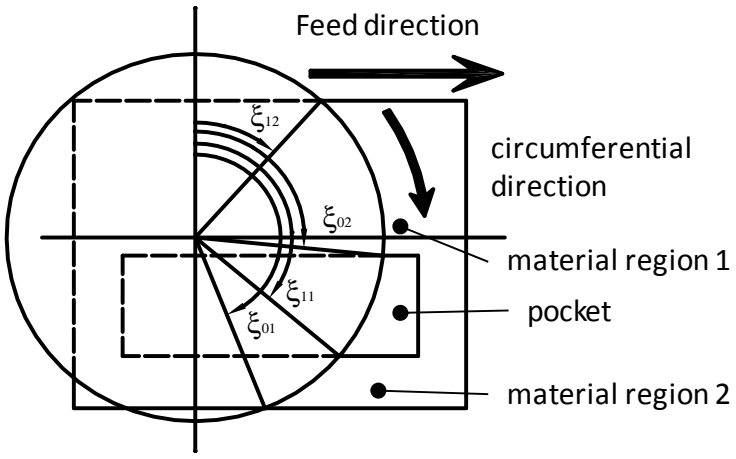

Figure 3-7 Cutter rotational angles [52]

Assume that the instantaneous center of velocity when the cutter-spindle system deflects is at point O in Figure 3-6. The distance from the datum to the spindle axis is *aR,* where *a* is a constant and *R* is the radius of the cutter. Then the moment of axial cutting force is

$$\begin{aligned} M_z &= P_z d.f_t \sum_{i=1}^{N} (\delta(\theta_i(t)) \sin\theta_i(t) R \sin\theta_i(t) + aR) \\ &= P_z d.f_t R \sum_{i=1}^{N} (\delta(\theta_i(t)) \sin^2\theta_i(t) + a) \end{aligned} \tag{3-4}$$

The average of moment of axial cutting force about a rotational angle of $(2\pi R)/N$ of the cutter is

$$\begin{aligned} \overline{M_z} &= \frac{N}{2\pi R} \sum_{\theta=\theta_0}^{\theta_m} P_z d.f_t R\Delta s \sum_{i=1}^{N} \delta(\theta_i(t))(\sin^2\theta_i(t) + a) \\ &= \frac{NP_z d.f_t R\Delta s}{2\pi R} \sum_{\theta=\theta_0}^{\theta_m} \sum_{i=1}^{N} \delta(\theta_i(t))(\sin^2\theta_i(t) + a) \\ &= C_z \sum_{\theta=\theta_0}^{\theta_m} \sum_{i=1}^{N} \delta(\theta_i(t))(\sin^2\theta_i(t) + a) \\ &= C_z V_z \end{aligned} \tag{3-5}$$

where θ_m (m=1,2…360) is the rotational angle of the cutter at step m, Δs is incremental angle (0.5 degree in this study). Given a constant depth of cut, feed rate, and cutting velocity, C_z is a constant defined as

$$C_z = \frac{NP_z d.f_t R\Delta s}{2\pi R} \tag{3-6}$$

Thus, this equation indicates that the cutting moment due to F_z is proportional to the geometrical parameters V_z. The cutting load or moment can be estimated by V_z. Considering the effect of a, V_z can further be decomposed as

$$V_z = V_{z1} + aV_{z2} \tag{3-7}$$

where V_{z1} and V_{z2} can be calculated by

$$V_{z1} = \sum_{\theta=\theta_0}^{\theta_m} \sum_{i=1}^{N} \delta(\theta_i(t)) \sin^2 \theta_i(t) \quad \text{and} \tag{3-8}$$

$$V_{z2} = \sum_{\theta=\theta_0}^{\theta_m} \sum_{i=1}^{N} \delta(\theta_i(t)) \tag{3-9}$$

where V_{z2} is the effect of distance a on the resultant moment around point O.

Horizontal cutting force in the feed direction on insert i is

$$F_{yi} = P_y C_i(\theta_i(\phi))d \tag{3-10}$$

where P_y is cutting pressure on inserts in Y direction. Moment caused by cutting forces in Y direction is

$$\begin{aligned} M_y &= P_y d.f_t \sum_{i=1}^{N} \delta(\theta_i(\phi)) \sin \theta_i(\phi) b \\ &= P_y df_t b \sum_{i=1}^{N} \delta(\theta_i(\phi)) \sin \theta_i(\phi) \\ \overline{M_y} &= C_y \sum_{\theta=\theta_0}^{\theta_m} \sum_{i=1}^{N} \delta(\theta_i(\phi)) \sin \theta_i(\phi) \\ &= C_y V_y \end{aligned} \tag{3-11}$$

where

$$C_y = P_y df_t b \text{ and} \tag{3-12}$$

$$V_y = \sum_{\theta=\theta_0}^{\theta_m} \sum_{i=1}^{N} \delta(\theta_i(\phi)) \sin \theta_i(\phi) \tag{3-13}$$

Similar to the z direction, the V_y is determined by surface geometry and can be used to approximate the cutting load/moment caused by F_y. By combining the loads induced by F_x and F_y, the resultant moment about point O is

$$M = C_z V_z - C_y V_y \tag{3-14}$$

Thus, the tilt angle and the deflection angle can be expressed as

$$\begin{aligned} \beta &= \beta_0 + \Delta\beta \\ &= \beta_0 + M / K \\ &= \beta_0 + (C_z / K) V_z - (C_y / K) V_y \\ &= \beta_0 + (1 / K_z) V_z - (1 / K_y) V_y \\ &= \beta_0 + (1 / K_z) V_{z1} + (1 / K_z) a V_{z2} - (1 / K_y) V_y \end{aligned} \tag{3-15}$$

where K is stiffness of spindle-cutter and K_z and K_y are determined by

$$\begin{aligned} K_z &= K / C_z = \frac{2\pi K}{N P_z d . f_t \Delta s} \\ K_y &= K / C_y = K / P_y df_t b \end{aligned} \tag{3-16}$$

where K_z and K_y are induced stiffness in Z and Y direction, respectively.

Model (3-15) reflects the impact of surface geometry and initial cutter tilt on the instant cutter tilt. Potentially, the parameters β_0, K_z, K_y can be used to monitor machine tool conditions. However, as the cutter is worn, cutting pressure P_z and P_y on inserts in model (3-16) increases, thus enlarging values of K_z and K_y. Such an increase potentially masks the true problem in the machine tool system. Therefore, tool life should also be incorporated into model (3-15).

To consider the effect of tool wear, we assume that the machine health parameters are constant during one cycle of tool life, e.g., K, a, b are constants. It is also assumed that the cutting pressure P_z, P_y is linear to remaining tool life t_{RTL} (in terms of percentage of a new tool life).

$$\begin{aligned} P_z &= P_{z0} + \alpha_{Pz}(100 - t_{RTL}) \\ P_y &= P_{y0} + \alpha_{Py}(100 - t_{RTL}) \end{aligned} \tag{3-17}$$

where P_{z0} and P_{y0} are the cutting pressure in Z and Y directions at the time when the inserts are new. The α_{Pz}, α_{Pz} are parameters that show the increase of cutting pressure on inserts when the remaining tool life is decreasing.

Substituting Eq. (3-17) into (3-16), we have

$$\begin{aligned} 1/K_z &= 1/K_{z0} + \mu_{Pz}(100 - t_{RTL}) \\ 1/K_y &= 1/K_{y0} + \mu_{Py}(100 - t_{RTL}) \end{aligned} \tag{3-18}$$

where $K_{z0} = \dfrac{2\pi RK}{NP_{z0}d.f_tR\Delta s}$; $\mu_{Kz} = \dfrac{N\alpha_{Pz}(100 - t_{RTL})d.f_tR\Delta s}{2\pi RK}$; $K_{y0} = \dfrac{2\pi RK}{NP_{y0}d.f_tR\Delta s}$;

$\mu_{Ky} = \dfrac{N\alpha_{Py}(100 - t_{RTL})df_tR\Delta s}{2\pi RK}$

Eq. (3-15) can then be expressed as

$$\begin{aligned} \beta &= \beta_b + (1/K_z)V_{z1} + (1/K_z)aV_{z2} - (1/K_y)V_y \\ &= \beta_b + [1/K_{z0} + \mu_{Kz}(100 - t)]V_{z1} + [1/K_{z0} + \mu_{Kz}(100 - t)]aV_{z2} - [1/K_{y0} + \mu_{Ky}(100 - t)]V_y \\ &= \beta_b + (1/K_{z0})V_{z1} + (1/K_{z0})aV_{z2} - (1/K_{y0})V_y + \varepsilon_\beta(100 - t_{RTL}) \end{aligned} \tag{3-19}$$

where, $\varepsilon_\beta = \mu_{Kz}V_{z1} + \mu_{Kz}aV_{z2} - \mu_{Ky}V_y$. Eliminating the effect of tool wear can lead to a more accurate estimate of the induced stiffness of the system. This model will be used to evaluate the initial cutter tilt β_0 and cutter-spindle stiffness (K_z, K_y) based on the HDM data.

3.3 Initial cutter tilt and cutter-spindle stiffness estimation based on HDM data

This section presents a statistical procedure to estimate β_0 and (K_z, K_y) in model (3-19). This is accomplished in four steps: (1) estimation of instant cutter tilt β from HDM data, (2) estimation of parameters V_z, V_y from workpiece geometry, (3) extraction of β_0 and (K_z, K_y) by statistical fitting the model to data (β; V_z, V_y), and (4) estimation of tool life effect. Figure 3-8 illustrates the procedure.

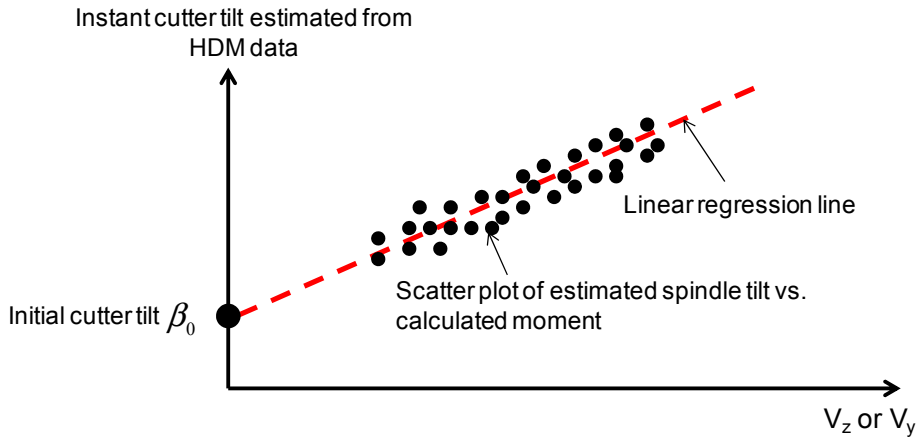

Figure 3-8 Illustration of initial cutter tilt and cutter-spindle estimation from HDM data

(1) *Estimation of instant cutter tilt*. Since the profile of toolmarks reflects the inclination of the tilting plane, this paper uses the tool mark profile to estimate the cutter tilt. Figure 3-9 illustrates the method of extracting tool mark data whereby surface data points between adjacent toolmarks are used to estimate the tilt plane through least square algorithm.

In practice, the toolmark captured by the LHI is caused by the wiper inserts for which the end cutting edges parallel the feed direction. Therefore, toolmark geometry that results from insert geometry can be ignored. For a large machined

surface such as engine head, several toolmarks can be used to estimate the corresponding tilting plane (Figure 3-9b). An example of estimated cutter tilt angle along feed direction of a machined surface is shown in Figure 3-10 which indicates that cutter-spindle deflection varies as the cutting proceeds due to varying cutting load induced by surface geometry.

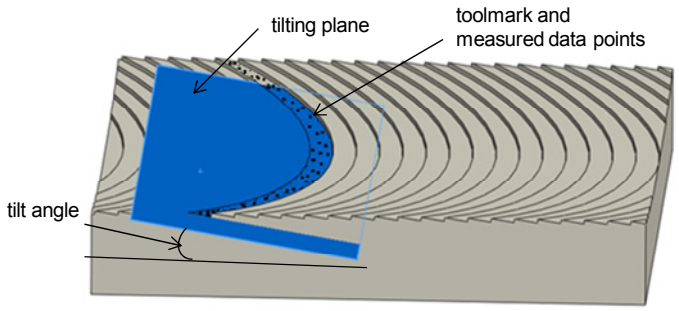

a) Estimating tilting angle at each toolmarks

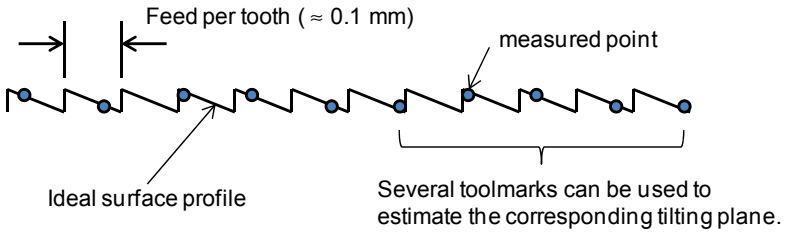

b) Estimating tilt angle using several toolmarks

Figure 3-9 Estimation of tilt angle a) Estimating tilt angle at each toolmark b) Estimating tilt angle using several toolmarks

Note: The workpiece often has large deformation at the cutting path entry as well as exiting areas, which affects the estimation accuracy. The data from these areas should be excluded from the calculation.

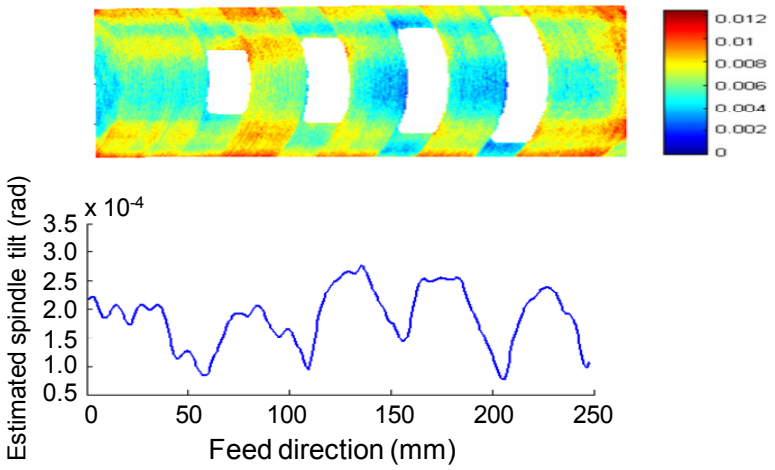

Figure 3-10 A machined surface and estimated cutter tilt angle along feed direction

(2) *Estimation of cutting load related parameters*. V_z, V_y reflect the impact of workpiece geometry on cutting forces. The parameters will be calculated using Eq. (3-8, 3-9, 3-13).

(3) *Statistical fitting*. Eq. (3-15) will be applied to the data to the following model.

$$\beta = b_0 + b_1 V_{z1} + b_2 V_{z2} - b_3 V_y + \varepsilon \tag{3-20}$$

The estimated coefficients are $\hat{b}_0, \hat{b}_1, \hat{b}_2,$ and $\hat{b}_3$. Then, $\hat{\beta} = \hat{b}_0, \hat{K}_z = 1/\hat{b}_1, \hat{K}_y = \hat{b}_3$.

(4) *Estimation of tool life effect*. With each set of surface data and given remaining tool life, the induced stiffness can be expressed as

$$\hat{K}_z(t_{RTL}) = (1/K_{z0} + \mu_{Pz} t_{RTL})^{-1}, \hat{K}_y(t_{RTL}) = (1/K_{y0} + \mu_{Py} t_{RTL})^{-1} \tag{3-21}$$

The induced stiffness without the effect of toolwear ($\hat{K}_{z0}, \hat{K}_{y0}$) can be obtained after fitting $\hat{K}_z(t_{RTL}), \hat{K}_{y0}(t_{RTL})$ into Eq. (18). These stiffness parameters reflect conditions of cutter-spindle assembly.

Note: The proposed method of extracting instant cutter tilt and cutter deflection does not consider the potential non-uniformity of workpiece deformation along each toolmark. However, this non-uniformity can be ignored when the workpiece is stiff and stably clamped. The deformation of worpiece does not generate a rotation of the plane between toolmarks, and thus does not affect estimations of the tilting plane angles.

3.4 HDM Based Spindle Condition Monitoring

This section discusses applications of the cutter tilt model in machine tool health monitoring. One method can be a direct comparison among the instant tilt angles estimated from different machines. However, the comparison result that intended to reflect machine difference could be confounded with the effects of cutting load differences induced by different surface geometry (part types). Therefore, it is more rational to monitor parameters (i.e., set up β_0, stiffness K_z and K_y) that reflect machine tool properties. As shown in Figure 3-11, machines with different initial spindle set-up or different stiffness could have the same instant cutter tilt. It is necessary to jointly monitor intercept (β_0) and slopes of curves (K_z, K_y).

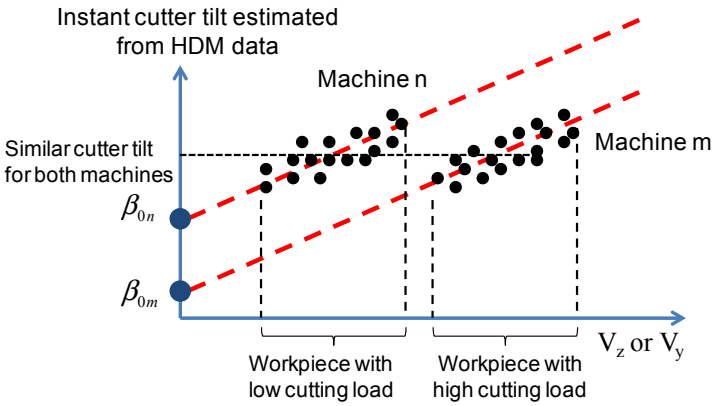

a) Two machines with different initial cutter tilt

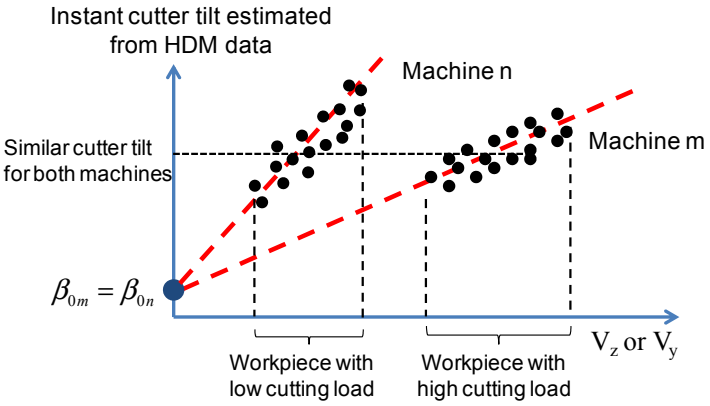

b) Two machines with different stiffness

Figure 3-11 Illustration of multi-machine monitoring

The correlation between the cutting load and instant cutter tilt should be inspected prior to monitoring the initial cutter tilt and induced stiffness. If the correlation is lost when certain special cause occurs in the system (such as loose ball screw bearing or tool breakage), the estimation of these parameters are not accurate.

Case study 1

This case study illustrates the monitoring method through an example of a face milling process that consists of four CNC machines (Machine 1-Machine 4) cutting the parts with four types of surface geometry designs (Figure 3-12). The Machine 4

produces part surfaces with backcutting tool marks. On each machine, a number of surfaces are measured across a range of tool life as shown in Table 3-1.

Table 3-1 Number of measured surfaces and corresponding range of tool life

	Machine 1	Machine 2	Machine 3	Machine 4
Number of sample	252	251	237	8
Range of tool life	65-85%	56-90%	61-100%	80-87%

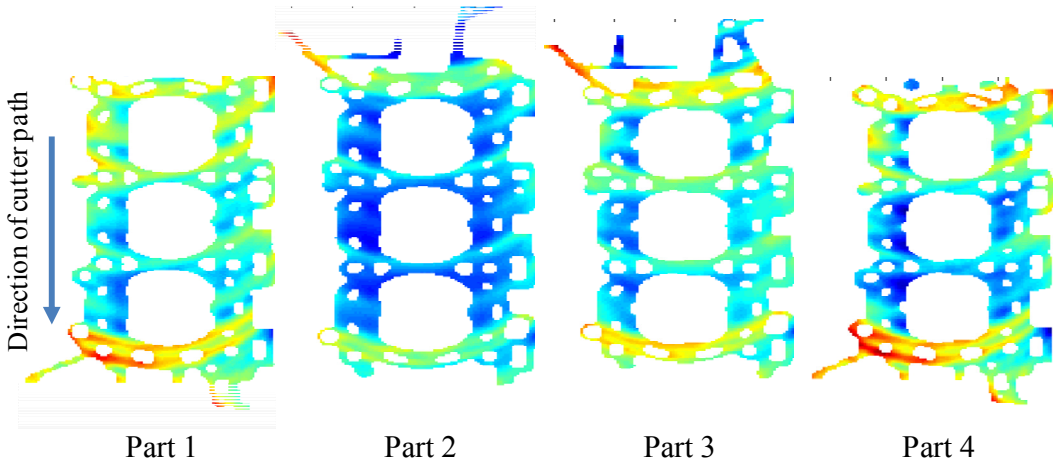

Figure 3-12 Four types of surface geometry machined at machines 1-4

Model validation

Following the procedures in Section 3, the instant cutter tilt and cutter load are estimated. Figure 3-13 is a scatter plot between the two parameters which shows a linear relationship. Thus, the result supports the model (3-15) and the assumption as shown in Figure 3-6.

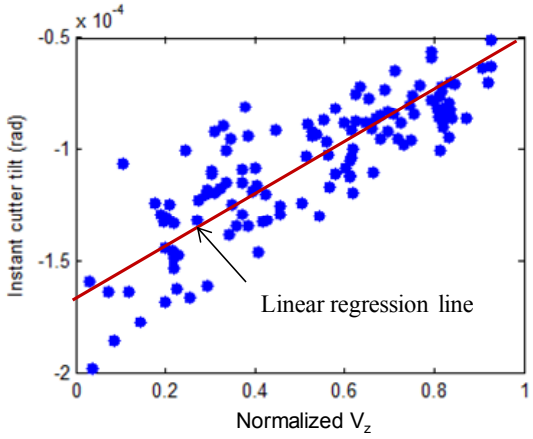

Figure 3-13 Scatter plot of cutter tilt vs. Mz of part type 1

Results of Estimated Machine Setup and Stiffness

The induced stiffness is first monitored. The K_z and K_y of the four machines are shown in Figure 3-14a and Figure 3-14b, respectively. By fitting Eq. (18) to the data of stiffness $K_z(t_{RTL})$, $K_y(t_{RTL})$, the original stiffness (K_{z0}, K_{y0}) with corresponding p-values can be obtained as shown in Table 3-2. It should be noted that Machine 4 produced parts with a short tool life span and the effect of remaining tool life cannot be precisely estimated. The data in Table 3-2 indicates that the tool life effect is insignificant on Machines 1 and 2 and significant on Machine 3. To explain this result, we notice that the remaining tool life data from machines 1 and 2 continuously span from 65% to 85-95% whereas the data from machine 3 cover two ends of the too life span and the data in a middle range between 65%-80% are missing. The remaining tool life in the middle range (65%-80%) on machines 1 and 2 has a large variation which potentially masks the real tool life effect. Therefore, the remaining tool life has an insignificant effect on these two machines but shows a negative effect on machine 3.

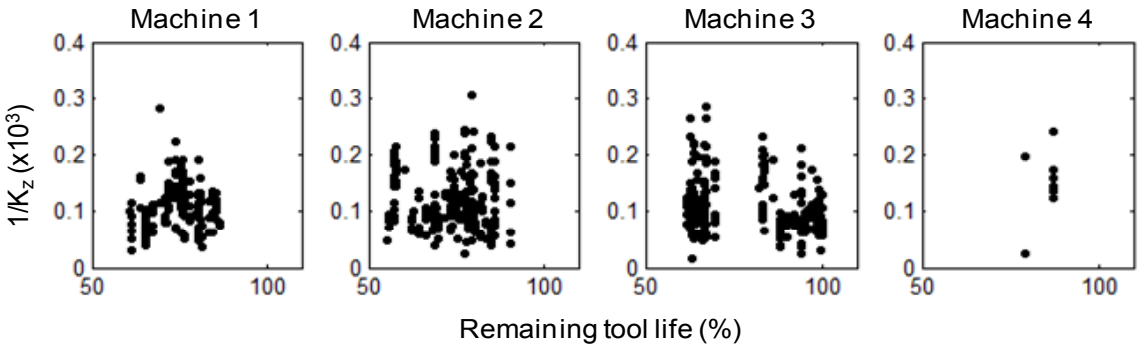

a) Stiffness of machines in Z direction

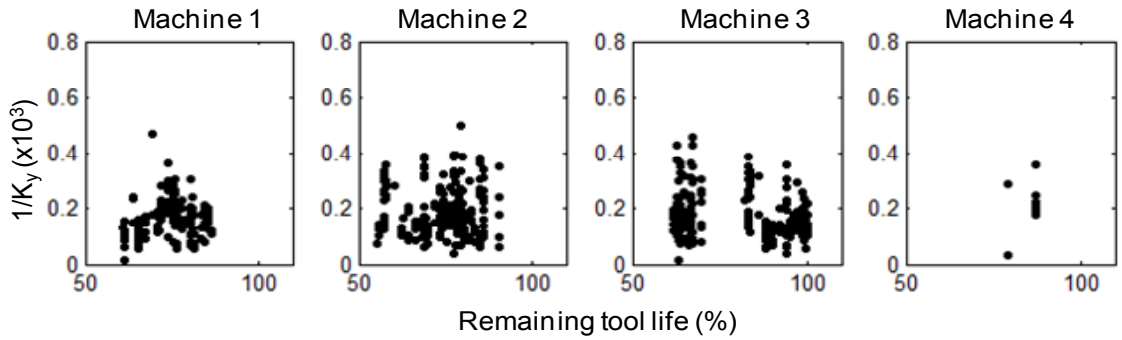

b) Stiffness of machines in Y direction

Figure 3-14 Stiffness of the machines in Y direction a) Stiffness in Z direction b) Stiffness in Y direction

Table 3-2 Induced stiffness of the machines and the influential factor of tool life

Parameters / Machines	$1/K_{0y}$	$1/K_{0y}$	μ_{0z}	μ_{0y}
Machine 1*	*75.4*	*96.4*	*0.0005*	*0.0009*
Significance (p-value)	*0.0292*	*0.0448*	*0.2995*	*0.2142*
Machine 2	155.9	243.0	-0.0005	-0.0008
Significance (p-value)	*2.3e-07*	*2.38e-06*	*0.354*	*0.458*
Machine 3	162.7	236.7	-0.0007	-0.0008
Significance (p-value)	*< 2.2e-16*	*< 2.2e-16*	*0.000657*	*0.0346*
Machine 4	-	-	-	-

* data collected from Machine 1 has short duration of remaining tool life; - the effect of tool life on Machine 4 cannot be precisely estimated

To further investigate the impact of tool life on the induced stiffness, the data for each machine were dived into two subgroups where the first group covers poor remaining tool life and the second covers the rest. Hypothesis testing was performed to compare the difference between the two subgroups. The results show that the remaining tool life has a significantly negative effect on induced stiffness on Machines 1 and 3 (Table 3-3) where K_{zi} and K_{yi} represent the induced stiffness for subgroup i, i=1,2. Therefore, the tool life impacts the variation of induced stiffness (K_z, K_y) in Eq. (3-18), especially when the tool is worn. It is necessary to consider this effect when monitoring machine health condition.

Table 3-3 The induced stiffness of the machines under different remaining tool life

Hypothesis / Machines	$H_0: 1/K_{z1} = 1/K_{z2}$	$H_0: 1/K_{y1} = 1/K_{y2}$
Machine 1	$\widehat{1/K_{z1}}$=122.6; $\widehat{1/K_{z2}} = 85.6$ p-value = 5.838e-10	$\widehat{1/K_{y1}} = 185.6$; $\widehat{1/K_{y2}} = 128.7$ p-value = 1.79e-08
Machine 2	$\widehat{1/K_{z1}} = 111.4$; $\widehat{1/K_{z2}} = 115.8$ p-value = 0.5057	$\widehat{1/K_{y1}} = 174.6$; $\widehat{1/K_{y2}} = 184.3$ p-value = 0.3892
Machine 3	$\widehat{1/K_{z1}} = 114.3$; $\widehat{1/K_{z2}} = 92.1$ p-value = 1.856e-05	$\widehat{1/K_{y1}} = 178.2$; $\widehat{1/K_{y2}} = 151.6$ p-value = 0.0022

Table 3-4 and Table 3-5 show statistical comparison among the induced stiffness of the four machines. For K_z, Machine 4 is significantly different from Machines 1-3; and for K_y, most of machines are consistent except Machine 4. Therefore, it can be seen that Machine 4 is significantly different from other 3 machines.

Table 3-4 p-values for comparing the KZ among the machines

Machines	Machine 1 $\widehat{1/K}_{z1}$=111.0	Machine 2 $\widehat{1/K}_{z2}$=114.1	Machine 3 $\widehat{1/K}_{z3}$=109.6	Machine 4 $\widehat{1/K}_{z4}$=148.8
Machine 1				
Machine 2	0.5029			
Machine 3	0.7448	0.2790		
Machine 4	0.0049	0.0451	0.0125	

Table 3-5 p-values for comparing the KY among the machines

Machines	Machine 1 $\widehat{1/K}_{y1}$=167.8	Machine 2 $\widehat{1/K}_{y2}$=180.4	Machine 3 $\widehat{1/K}_{y3}$=176.0	Machine 4 $\widehat{1/K}_{y4}$=215.1
Machine 1				
Machine 2	0.1046			
Machine 3	0.2404	0.5200		
Machine 4	0.0330	0.2357	0.1367	

Figure 3-15 shows the monitoring results of the initial cutter tilt β_0 calculated by Eq. (3-15). Table 3-6 compares the estimated initial angle of these machines. It can be seen that Machines 1 and 3 have consistent initial cutter tilt angles. Machine 2 has a significantly higher initial cutter tilt whereas Machine 4 has a significantly smaller cutter tilt. This result indicates that Machine 4 can create back-cutting tool marks on surfaces as is consistent with the data from the machining process. The reason can be illustrated by Figure 3-15 that compares machines with different initial spindle set-up. A less negative initial cutter tilt will lead to an instant cutter tilt that is close to zero (back-cutting limit in Figure 3-16) under cutting load, thus making it more likely to generate back-cutting tool marks.

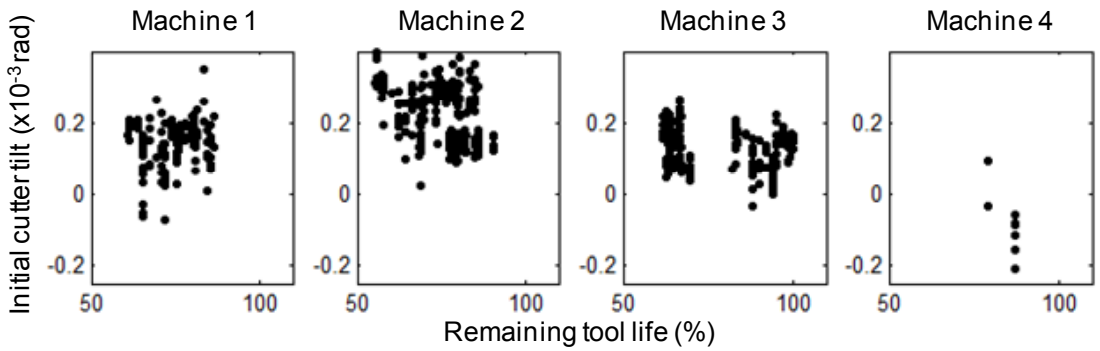

Figure 3-15 Cutter tilt of four machines

Table 3-6 p-values for comparing the β0 among the machines

Machines	Machine 1 $\hat{\beta}_{01} = 0.1435\text{e-}3$	Machine 2 $\hat{\beta}_{02} = 0.2378\text{e-}3$	Machine 3 $\hat{\beta}_{03} = 0.1389\text{e-}3$	Machine 4 $\hat{\beta}_{04} = -0.0815\text{e-}3$
Machine 1				
Machine 2	< 2.2e-16			
Machine 3	0.3930	< 2.2e-16		
Machine 4	< 2.2e-16	< 2.2e-16	< 2.2e-16	

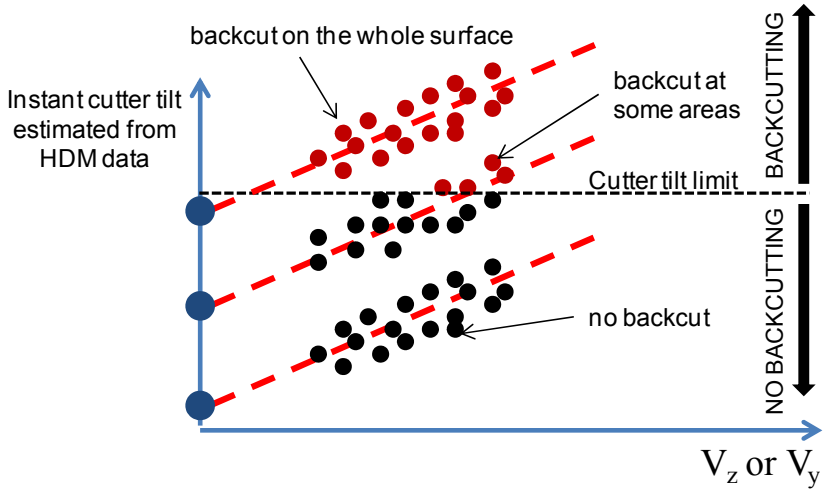

Figure 3-16 Instant cutter tilt and back-cutting

Case study 2

One machine has a problem of loose ball screw bearing in spindle assembly; on a machine the remaining tool life on this machine is around 85%. Data was collected prior, during, and after the problem. The induced stiffness K_{Z0} is calculated and shown in Figure 3-17. This indicates that the induced stiffness significantly changes because the relationship between moment of cutting forces and cutter tilt changed when the ball screw bearing looseness occurred. Such a change can be detected by performing a Pearson correlation test on the the spindle tilt and correlation between estimated spindle tilt β and cutting moment related quantity V_z. When the correlation r is close to 0, a loose ball screw problem is more likely to occur. To test this statement, a hypothesis can be performed on H_0: r=0 vs. H_1: r>0 or H_1: r<0. Pearson correlation testing can be used by comparing a test statistic $t = \hat{r}\sqrt{\frac{n-2}{1-\hat{r}^2}}$ with the 100(1-α)% percentage point $t_{1-\alpha, n-2}$, where $\hat{r}$ is the estimated Pearson correlation from samples.

The statistical test was implemented based on the data as shown in Fig. 18. Under normal conditions (left panel), it was found that estimated Pearson correlation coefficient r is negative (accept H_1) whereas when the loose ball screw problem occurred, r=0 (accept H_0, no significant correlation presents, see the right panel).

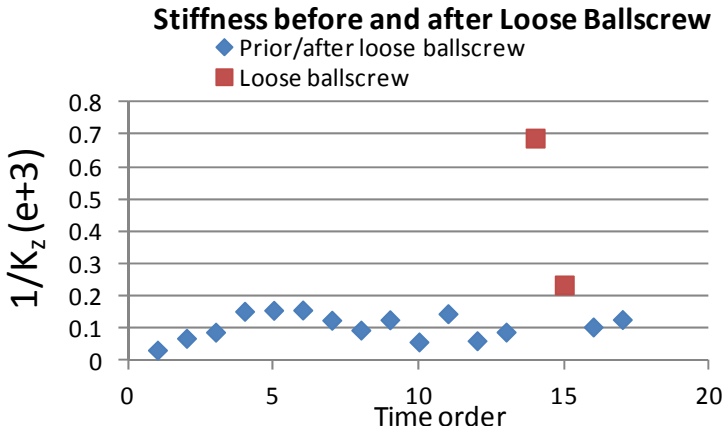

Figure 3-17 The change of system stiffness when loose ball screw bearing happens

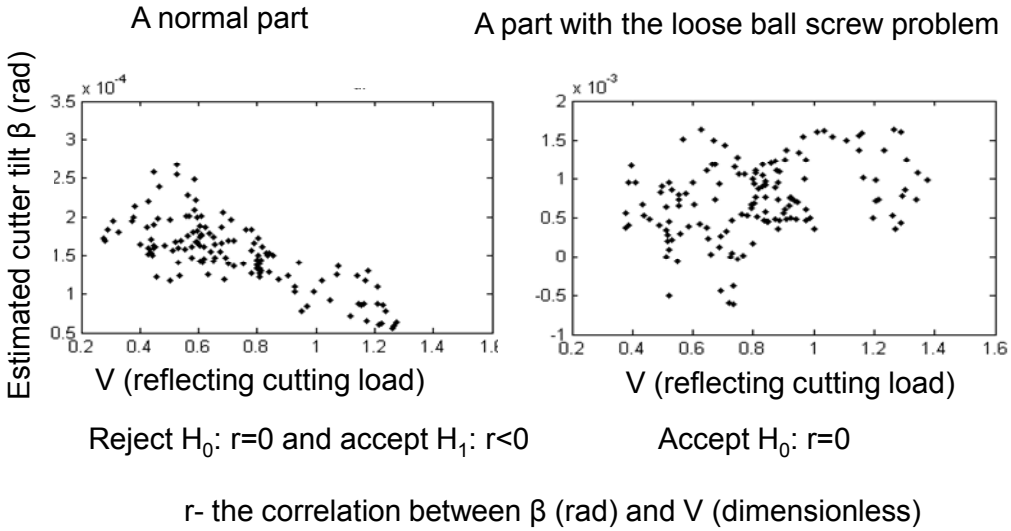

Figure 3-18 Spindle tilt- cutting load correlation vs. loose ball screw problem

3.5 Conclusions

This chapter models the impact of cutting force induced moment on cutter-spindle deflection during face milling and thereby develops a method of using HDM data to monitor machine conditions including initial cutter tilt and cutter-spindle system stiffness. The cutting force model links the instant cutter tilt with initial cutter tilt and

cutter-spindle stiffness by considering both cutting force variation induced by surface geometry and the effect of tool wear. To obtain the model parameters, the HDM data are employed to (1) estimate the instant cutter tilt by fitting a tilting plane to the data between adjacent tool marks and (2) estimate the cutting load from surface geometry. The initial cutter tilt and cutter-spindle stiffness are estimated by fitting the established model to the estimated instant cutter tilt and cutting load through the linear regression. This method directly extracts the instant cutter tilt from the HDM data and has the advantage of improving estimation accuracy when the machined surface has complex geometry such as holes or asymmetry. Monitoring the initial cutter tilt provides information on machine setup and monitoring the cutter-spindle stiffness reveals machine tool conditions such as loose/worn bearing on spindle assembly or ball screw. The paper also discusses monitoring procedures, i.e., the correlation between the cutting load quantity and the instant cutter tilt should be inspected first; and monitoring of the initial cutter tilt and induced stiffness are implemented only when the correlation is strong. Two case studies demonstrated the effectiveness of the developed method based on the HDM data collected from a Ford engine plant.

CHAPTER 4

SURFACE VARIATION REDUCTION FOR FACE MILLING USING HIGH-DEFINITION METROLOGY

This chapter develops a face milling process planning method to reduce surface height variation using the high definition metrology. The previous Chapters has found and established relations between variation patterns and cutting forces and associated process variables. Based on the findings, this paper compares potential machining methods and finds that the approaches of varying feed rate and the cutter path planning are most feasible for surface quality control. By combining the two approaches, an algorithm is developed to reduce cutting force variation along the feed direction and circumferential direction, respectively, thereby reducing the surface variation. A case study based on a cutting experiment is conducted to demonstrate the proposed machining method which improves the surface flatness by 25%. The varying feed method can effectively eliminate the surface variation along the feed direction while the optimal cutter path approach balance the cutting loads on the two sides of the cutter path.

4.1 Introduction

In the previous chapters, the relations between surface variation patterns and process parameters/variables that impact cutting force has been established. Through the cutting force model based surface characterization, the critical surface variations include: (1) global shape, (2) cutter-workpiece relative displacement induced variation, and (3) cutter-spindle deflection.

Global shape on machined surface (Figure 4-1a) is produced by overall deformation of workpiece under pressure of cutting forces. The shape has hammock form. Depending on stiffness of workpiece, the depth may vary. Figure 4-1a shows a hammock shape on engine head. The overall flatness of the hammock shape can be up to 20 μm, contributing about 30% of overall flatness of the machined surface, depending on varying tooling conditions.

As studied in Chapter 2, cutter-workpiece relative displacement contributes significant impact on surface height variation (Figure 2b and Figure 4-1b). Variation of cutting forces due to workpiece complexity along cutter path causes relative displacement between cutter and workpiece that produces a pattern of surface variation. That is surface height variation is linear to material removal rate in straight cuts. Surface height variation is also caused by cutter-spindle deflection (Chapter 3). Due to imbalance of cutting forces along cutter path, the deflection of cutter-spindle is also varied and contributes to surface height variation along cutter path (Figure 4-1c).

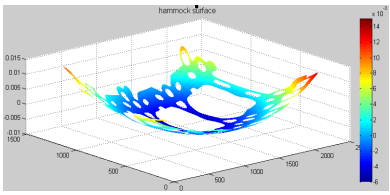

a) Global shape of an engine head

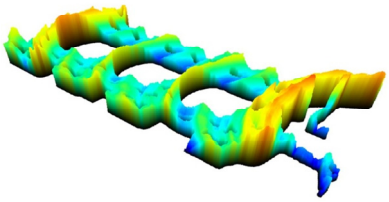

b) Surface variation in feed direction

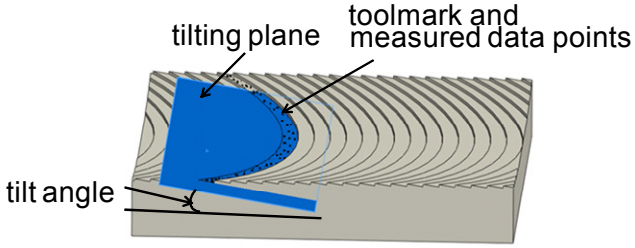

c) Cutter-spindle deflection induced surface variation

Figure 4-1 Surface height variation patterns

Research has been conducted to reduce surface errors on machined surface in ball-end milling [55-57]. There are a number of studies that improved fine surface quality such as roughness. De Meter developed a load model for optimizing fixture performance to reduce workpiece displacement [58] and introduced fast support layout optimization for machining fixture to increase workpiece rigidity to minimize workpiece deformation during machining [59]. Nee, A.Y.C. et al. [60] introduced a fixturing approach using sensory feedback and online fixturing control strategy for workpiece quality improvement with experiments on thin-walled workpieces. Other different strategies of workpiece fixturing, considering clamping force dynamics and thermal effect, were also studied [12, 61-65]. Surface height variation reduction has rarely been applied in face milling processes due to a lack of efficient measurement system that can provide a holistic view of a large surface. In addition, most of the research focuses on real-time adjustment of machine tool related operating parameters,

which requires additional installation of in-line sensors and control actuators. A cost-effective method for surface variation control based on routine surface inspection is highly desired to reduce surface variation.

Candidate machining methods to reduce surface variation are introduced in Section 4.2. Two methods that show the feasibility are varying feed rate and cutter path planning. In section 4.3, an algorithm of minimizing areal cutting force variation by jointly adjusting cutter path and feed rate is developed based on cutting force models along the feed direction and circumferential directions. In the circumferential direction, cutting load balancing is implemented. A case study based on face milling experiments will be presented to demonstrate the approach in Section 4.4. Conclusions will be given in Section 4.5.

4.2 HDM Based Surface Variation Reduction

In this section, several trial methods of surface variation reduction will be introduced and judged. Discussion will be follow to select the feasible methods. As mentioned in Chapter 2, relative cutter-workpiece displacement (including cutter-spindle deflection) produced surface variation patterns on the surface. The varying displacement is caused by varying cutting force and cutting force is related to MRR. Therefore, by controlling MRR, relative cutter-workpiece displacement can be controlled and surface variation can be reduced. To control MRR, the following parameters can be controlled: (1) depth of cut, (2) feed rate, (3) spindle speed, and (4) cutter path.

Depth of cut Depth of cut can be varied by moving cutter in axial direction. But the movement of a cutter would cause gouging issue, leaving sharp marks on the machined surface as shown in Figure 4-2.

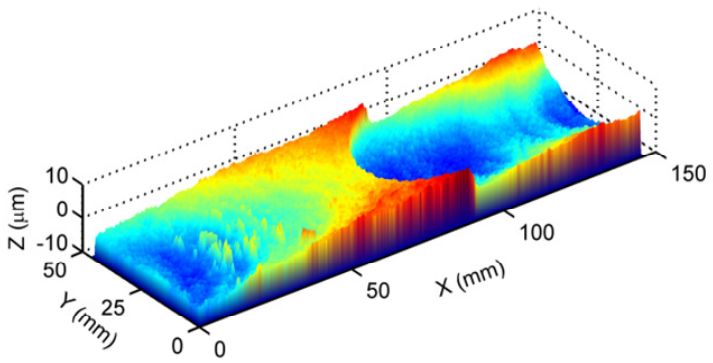

Figure 4-2 Gouging due to moving cutter in axial direction [66]

Feed rate To examine the idea of reducing surface variation by varying feed rate. The experiment simulate cutting of engine head at smaller scale. In order to keep MRR constant along cutter path, the feed rate is varied. In practice, the feed rate can not change continuously. Therefore, a stepwise feed rate variation is programmed. The cycle time may increase due to feed rate variation. Some feed rate compensation may be needed to keep cycle time constant. The results are shown in Fig. 4-3 and 4-4.

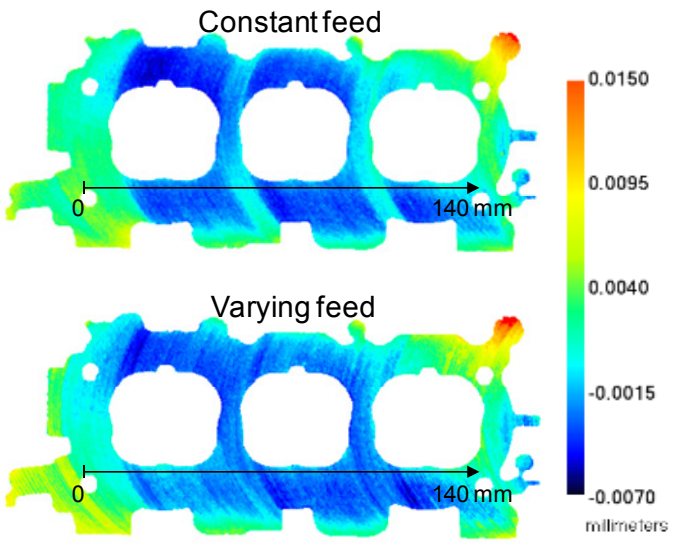

Figure 4-3 Comparison between machined surfaces of constant feed rate and varying feed rate

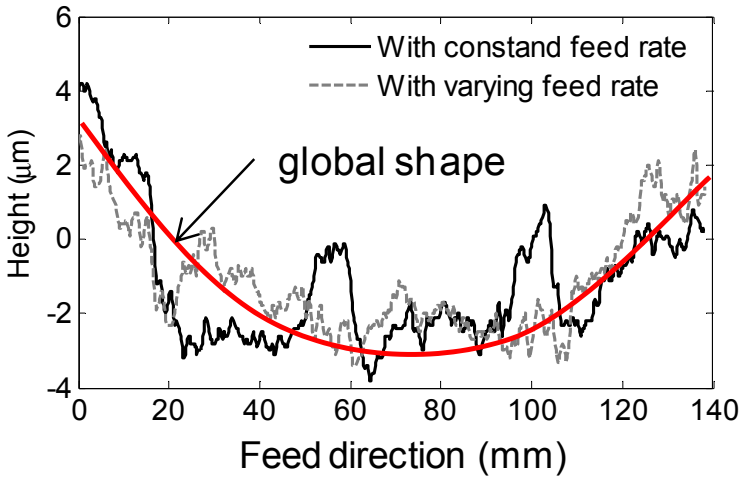

Figure 4-4 Comparison between surface height of constant feed rate and varying feed rate

Cutting velocity MRR also can be controlled by varying spindle speed. However, CNC machines nowadays changes speed very fast. That would lead to dynamic problems. For

example, due to dynamic change, a mark was created on the surface as shown in Figure 4-5. This mark would lead to leaking in assemblies.

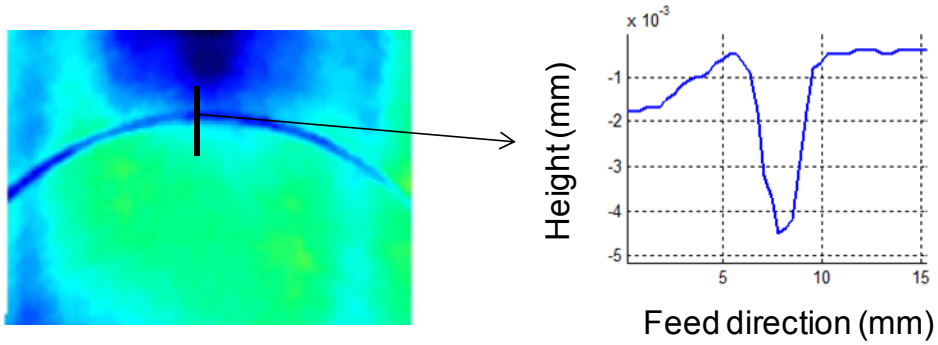

Figure 4-5 Machined surface when spindle speed is changed suddenly

Cutter path The original cutter path that was used to machine engine head block produces high variation of cutting load at the entry (Figure 4-6). The cutter path is optimized to reduce cutting load variation by changing cutter location to minimize the variation of MRR along cutter path. The optimized cutter path produces surface that is 22.5% flatter than the original surface.

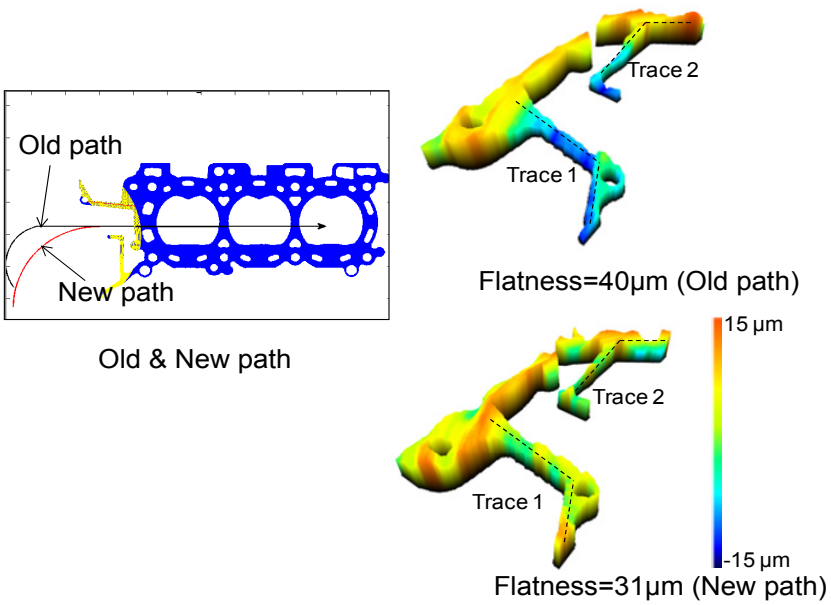

Figure 4-6 Original and the optimized cutter entry path

From the above experiments, it is obvious that changing MRR by varying feed rate and cutter path can effectively improve surface flatness without introducing additional surface local defects. Thus, the two approaches are mostly feasible to redistribute cutting load that would reduce surface variation. The following sections will focus on these methods.

4.3 Optimal machining planning algorithm through cutting force variation reduction

In this section, an algorithm of balancing cutting loads along cutter path as long as on both side of cutter path will be introduced. This approach focuses on the cutting force variations along the feed direction and cutting load imbalance on two sides on the cutter path. The cutting force variation along the feed direction has been modeled in Chapter 2. In this section, the cutter load balancing problem is discussed in detail.

Cutter load balancing on two sides of cutter path

Equations used to calculated moment of axial cutting force were introduced in Chapter 2 as follows,

$$\overline{M_z} = \frac{N}{4\pi R}\sum_{\theta=\theta_0}^{\theta_m} P_z d.f_t R\Delta s \sum_{i=1}^{N} \delta(\theta_i(t))\sin 2\theta_i(t)$$
$$= \frac{NP_z d.f_t \Delta s}{4\pi}\sum_{\theta=\theta_0}^{\theta_m}\sum_{i=1}^{N} \delta(\theta_i(t))\sin 2\theta_i(t)$$
$$= C_z V$$

To evaluate the balance of axial cutting load on both side of cutter path, a new parameter is introduced,

$$V = |V_R - V_L|, \tag{4-1}$$

where V_R and V_L are parameters that describe cutting load on the right and left of cutter path respectively as shown in Figure 1-1.

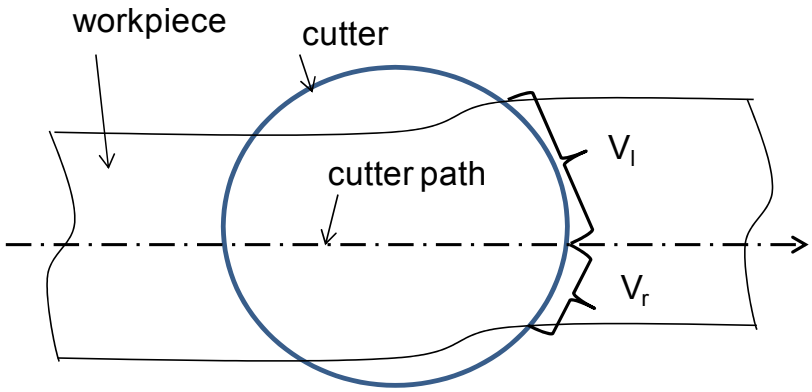

Figure 4-7 Cutting load balancing

Algorithm of optimizing cutter path and feed rate

To balance cutting load along cutter path and on both sides of cutter path, the cutter path and feed rate can be found from the optimization equations below,

Objective function:

$$\text{Min } \Delta a(S(x,y), f_r(x,y), G(x,y)) \tag{4-2}$$

$$\text{Min } \Delta V(S(x,y)) \tag{4-3}$$

Constraints:

$$F_{min} < f_r < F_{max} \tag{4-4}$$

$$T_{straight\_path} - \Delta T < T_{optimal\_path} < T_{straight\_path} + \Delta T \tag{4-5}$$

$$S'(x,y,t) < S_0 \tag{4-6}$$

where, Δa is the variation of MRR along cutter path $S(x,y)$ and varying feed rate $f_r(x,y)$ and taking into account the global shape $G(x,y)$, ΔV is the variation of parameter V along cutter path, F_{min}, F_{max} are minimum and maximum feed rates (varying feed rate too much would cause variation of surface roughness and waviness), $T_{straigh\_path}$ is the cycle time of each cut of straight cutter path, ΔT is time tolerance that is possible for increasing or decreasing cycle time of optimized cutter path, S_0 is maximum diversion angle of cutter path.

Summary: The proposed machining method will assist reducing surface variation pattern 1 (MRR induced surface variation), 2 (cutting load imbalance induced surface variation), and 3 (global shape) at the same time by varying feed rate and planning cutter path.

4.4 Case Study

This section demonstrates the proposed surface variation reduction strategy using a face mill experiment. The workpiece is shown in Figure 4-8. The cutting area is 1 mm higher than the remaining area as shown in Figure 4-8. The approximated dimension of cutting area is shown in Figure 4-9.

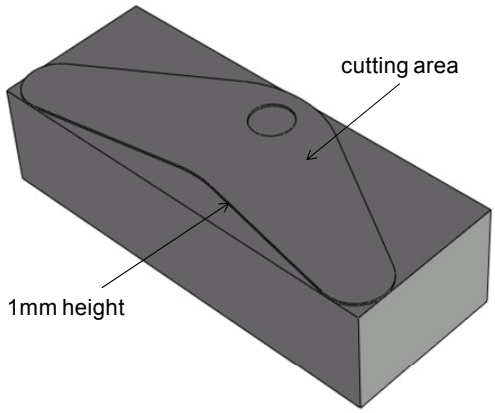

Figure 4-8 Solid Aluminum block and the cutting area

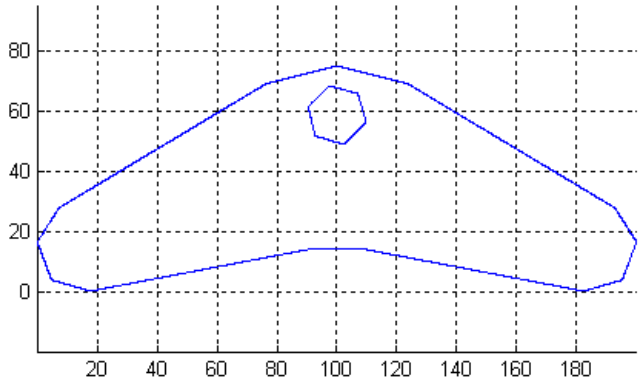

Figure 4-9 Geometry of cutting area

The workpiece is also designed to remove the effect of global shape. The global shape is estimated by fitting second order surface to measurement data of the whole face of the block. The flatness of the global shape is about 3 μm and the shape along feed direction is shown in Figure 4-10. As shown in Figure 4-4, the global shape has a significant impact on surface shape and it is necessary to eliminate it. In this experiment, the global shape is removed by a design of surface geometry that can adjust MRR to compensate for the quadratic surface shape as shown in Fig. 4-10. The MRR produced by a straight cutter path is shown in Figure 4-11a that will produce surface height

variation shown in Figure 4-11b. The MRR induced surface height variation is estimated based on MRR-surface height correlation (as discussed in Chapter 2). The combination of global shape and MRR induced surface height will reduce the height difference between the entrance/exit areas and middle section of the part.

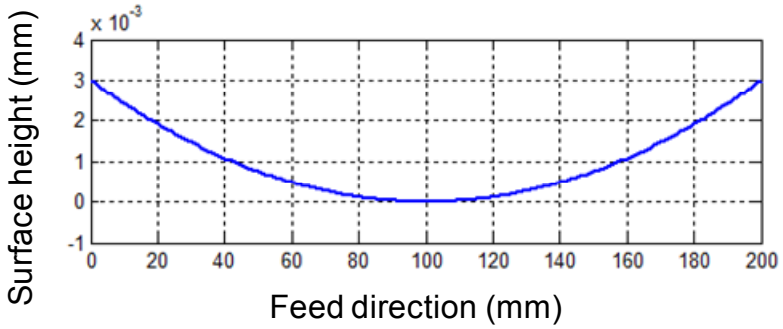

Figure 4-10 Estimated global shape

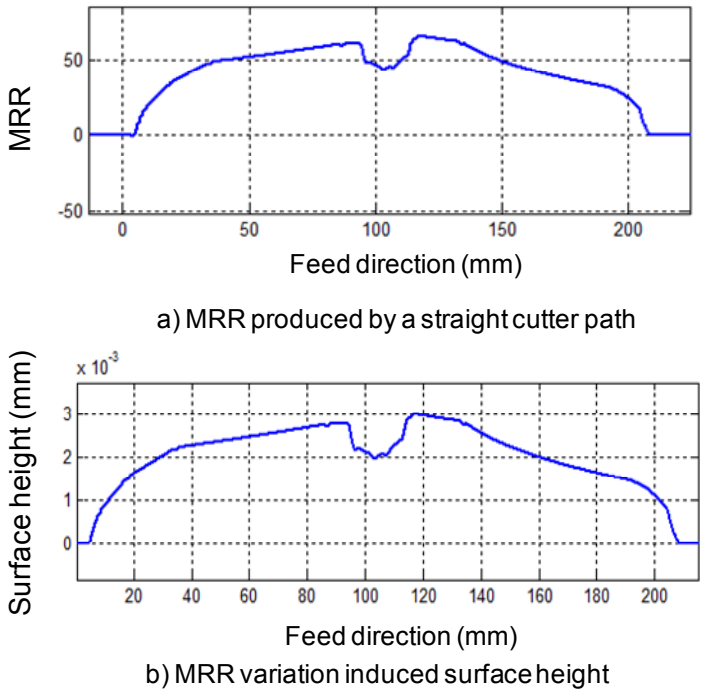

Figure 4-11 MRR and estimated surface height of straight cutter path

One more factor that contributes to surface height variation is cutting load imbalance. As seen in Figure 4-12, the difference between cutting load on two sides of the cutter path V, especially at areas I and III, will create surface variation along circumferential direction as shown in Figure 4-13 (feed rate of 0.1 mm/tooth).

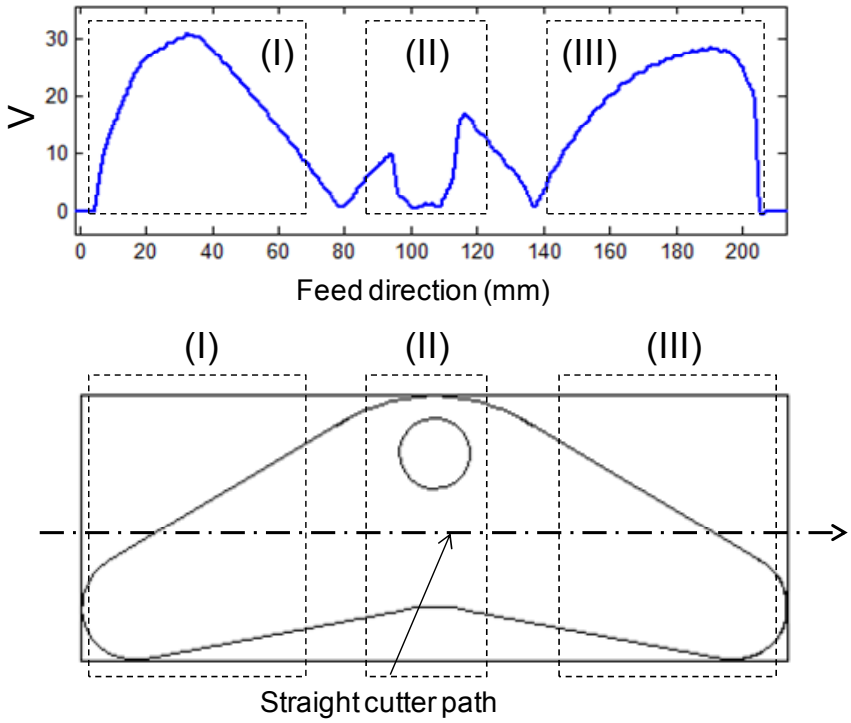

Figure 4-12 Cutting load imbalance produced by straight cutter path

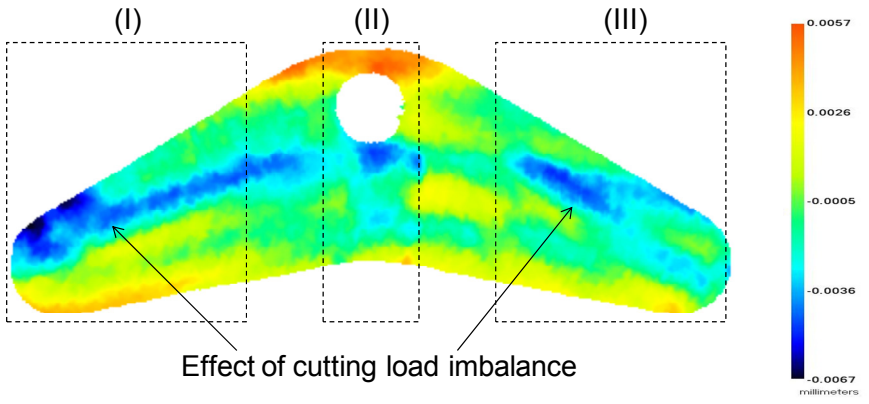

Figure 4-13 Machined surface produced by straight cutter path

Based on the algorithm developed in Section 4.3, cutter path and feed rate will be adjusted to deal with MRR variation along the feed direction and cutting load imbalance.

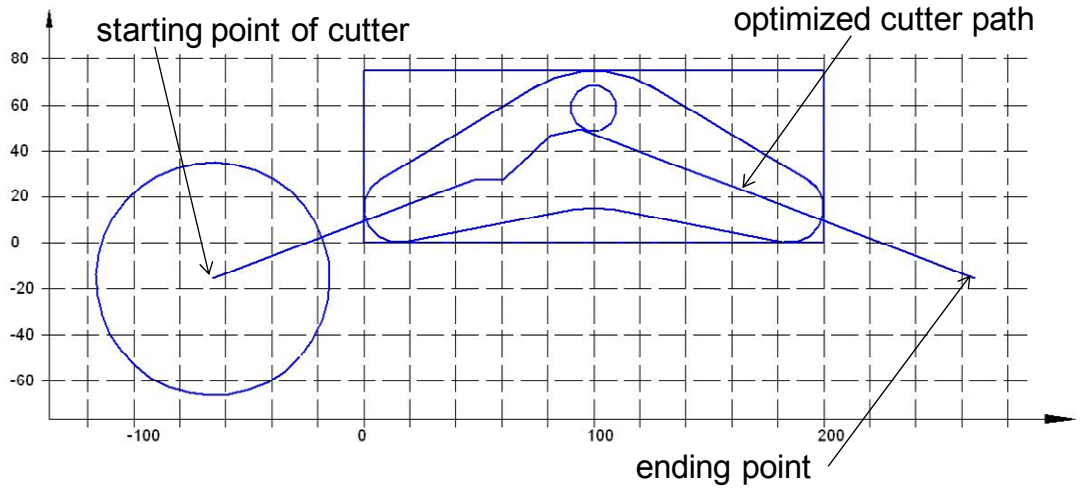

Figure 4-14 Optimized cutter path

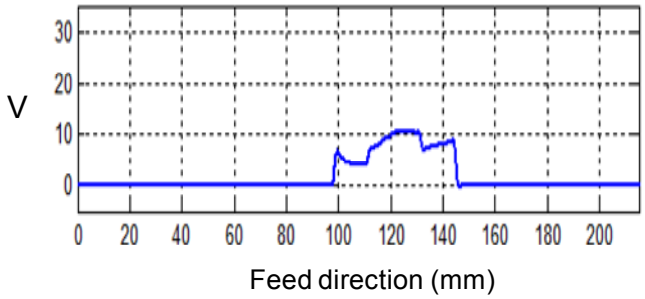

Figure 4-15 Parameter V along feed direction of optimized cutter path

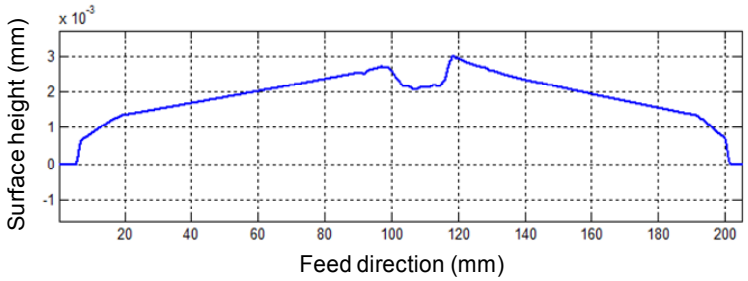

Figure 4-16 MRR variation induced surface height of optimized cutter path

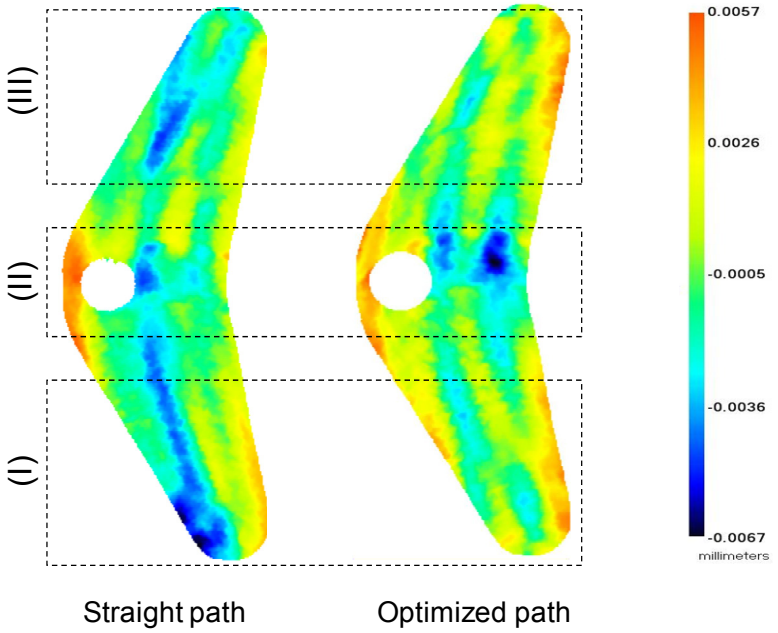

Figure 4-17 Machined surface produced by optimized cutter path with constant feed rate

To balance the cutting load in circumferential direction the cutter path should be optimized using Eq. (4.3-4.6) with F_{min} =0.07 mm/tooth, F_{max} =0.13 mm/tooth, ΔT = 0.1T, $S_0 = 45^0$. The optimized cutter path is shown in Figure 4-14 with constant feed rate of 0.1084 mm/tooth. The parameter V along feed direction of the optimized cutter path is shown in Figure 4-15 with smaller magnitude compared to the case of straight cutter path. The corresponding machined surface is shown in Figure 4-17. It is obvious that the surface height variation in circumferential direction at two ends is reduced

significantly. The remaining factor that causes low flatness is the MRR variation at the hole.

To jointly reduce the effect induced by cutting load imbalance and MRR variation, Eq. (4.2-4.6) will be used to optimize feed rate along feed direction. The feed rate at area II (surrounding the hole) is found to be 0.133 mm/tooth and the corresponding machined surface is shown in Figure 4-19. The effect of MRR variation at area II is significantly reduced.

The values of flatness of machined surface that are produced by three different cutter paths are given Table 4-1. It can be seen that the overall flatness of the surface is reduced by 25%. The height distributions of the three surfaces are compared in Figure 4-21. The result indicates that the method of optimized path along with varying feed rate yield the smallest surface height variation.

It should be noted that the surface cut by the optimized cutter path and feed rate still show a “high-low-high” variation patterns as shown in Fig. 4-20. As mentioned in Chapter 2, this pattern results from insert engagement patterns which are more significant when the cutter is small with fewer inserts. The patterns will be removed or less significant by employing more inserts.

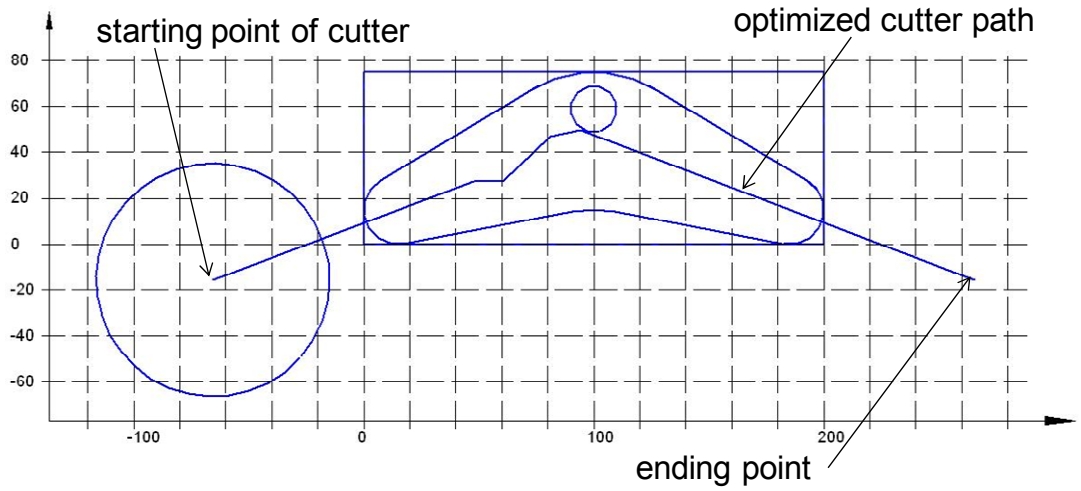

Figure 4-18 Optimized cutter path

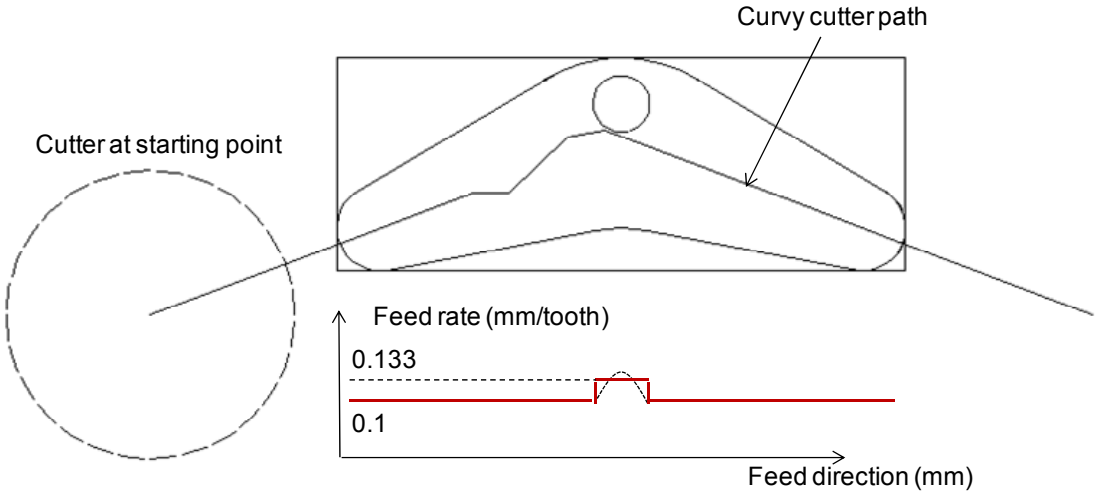

Figure 4-19 Varying feed on optimized cutter path

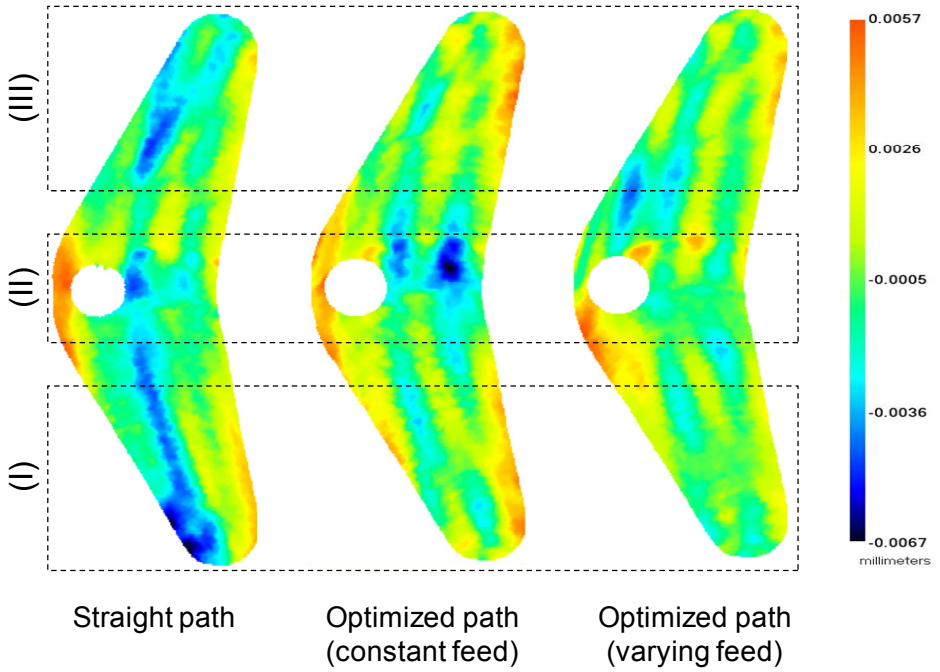

Figure 4-20 Machined surface of optimized cutter path with varying feed rate

Table 4-1 Comparison of machined surfaces

Cutter paths	Overall flatness (μm)	Variance of surface height distribution
Straight	12.3	0.0018
Optimized (constant feed)	11.9	0.0013
Optimized (varying feed)	9.6	0.0011

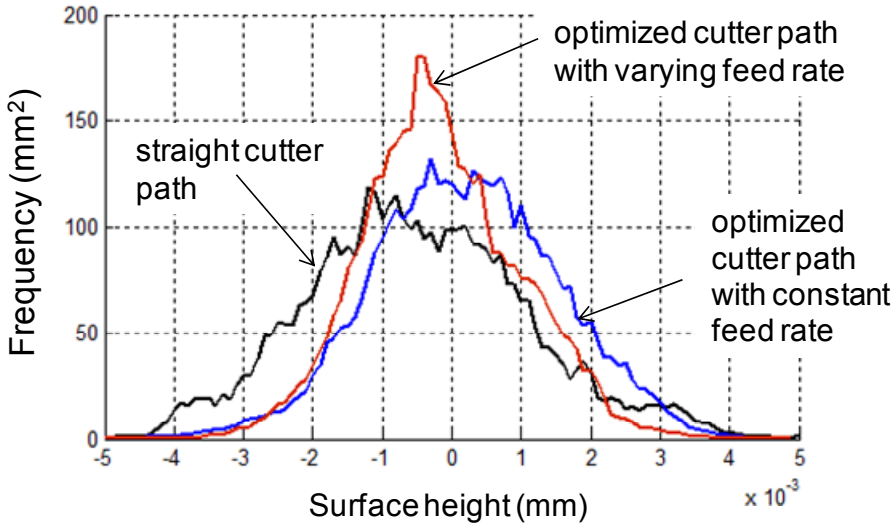

Figure 4-21 Comparison of surface height distribution for different cutter path

4.5 Conclusions

This chapter introduces a strategy to reduce surface height variation in face milling operation based on the observations from HDM data. Through cutting force modeling, our prior research on surface variation characterization based on HDM has uncovered and generation mechanisms for three types of surface patterns, i.e., (1) MRR induced surface variation, (2) cutting load imbalance induced surface variation, and (3) global shape. The proposed strategies aims to reduce the areal variation in cutting force distribution to reduce these surface variation patterns. The general strategies can be summarized as follows. The method of changing feed rate and/or cutter path can be used to compensate for the MRR induced surface variation. The method of optimizing cutter can reduce the cutting load imbalance induced surface variation in the circumferential direction. The global shape can be compensated for by reducing the MRR variation via varying feed rate method.

The case study based on a face milling experiment was conducted to demonstrate the applications of these strategies in reducing MRR induced surface variation and cutting load imbalance induced surface variation. The effect of global shape is first offset by a careful design of surface geometry. The machined surfaces profiles before and after applying the algorithms were compared and the result show that the proposed approach can significantly reduce the surface variation by 38% and overall surface flatness by 25%.

CHAPTER 5

SUMMARY AND FUTURE WORK

5.1 Summary

This thesis has established a methodology for characterizing and reducing surface variation using High Definition Metrology (HDM). An engineering-driven method was developed to improve surface characterization for process monitoring and control by combining cutting force modeling and HDM data. The approach leads to discovery of new surface variation patterns and their generation mechanisms. This thesis also exploited new applications of these patterns on process condition monitoring/diagnosis and cost-effective surface variation reduction method. A detailed summary of this thesis is given below.

1. *Model of axial cutting force induced cutter-workpiece relative displacement*

The impact of axial cutting force on surface variation was found in circumferential and feed directions. In the circumferential direction, it is found that surface profiles are correlated to the axial cutting force variation or cutter insert engagement. At the boundary where the number of inserts engaged in cutting changes, cutting force changes abruptly and results in jumps in the profile. This pattern is found to be sensitive to changes in cutter-workpiece system dynamics such as vibrations induced by clamping errors. In the feed direction, it is found that surface

variations are attributed to axial cutting force changes caused by MRR variations due to the complexity of surface geometry. The change of cutting force due to MRR variation causes relative displacements between cutter and workpiece, thus producing surface height variation. These findings will lead to important insights on surface design, process monitoring and improvement by maintaining a constant rate of material removal.

2. *Model of cutting force moment induced cutter-spindle deflection*

The impact of cutting force induced moment on cutter-spindle deflection during face milling in conjunction with HDM data was found and a method for monitoring machine conditions including initial cutter tilt and cutter-spindle system stiffness was thereby developed. The cutting force model links the instant cutter tilt with initial cutter tilt and cutter-spindle stiffness by considering cutting force variation induced by surface geometry and the effect of tool wear. To obtain the model parameters, the HDM data cloud is first utilized to estimate instant cutter tilt by fitting a tilting plane to the data between adjacent tool marks and estimate the cutting load from surface geometry. The initial cutter tilt and cutter-spindle stiffness is then extracted by fitting the established model to the estimated instant cutter tilt and cutting load through linear regression. The proposed method of directly extracting the instant cutter tilt from HDM data results in a reliable estimation when the machined surface has complicated geometry such as holes or being asymmetric.

3. Surface variation reduction of face milled surface by cutting load balancing

The proposed approach of reducing surface height variation was proven to be efficient in reducing surface variation patterns produced by global deformation, cutting load variation along feed direction (MRR variation), and cutting load imbalance on both sides of cutter path. The

purpose of this algorithm is to redistribute cutting load in the feed direction and circumferential direction of the cutter by optimizing cutter path and feed rate along cutter path. The approach work well when the cutter size and number of inserts are large.

4. *Summary of practical contributions*

The models established in this thesis lead to improved metrics of evaluating machined surface shape (such as surface variation in feed direction in face milling or back cutting caused by small spindle tilt) for automotive powertrain production. The new metrics can be used for process monitoring such as tooling conditions, machine stiffness, and cutter-spindle tilt. The proposed method of cutter path planning and cutting condition optimization has been partially implemented in a Ford engine plant which reports a surface flatness improvement by 15-25%. The methodology can improve quality and reduce cost.

5.2 Future work

With the rich data of large machined surfaces, there are still a lot of studies needed to further understand surface variation at the process level as well as at system level. The areas that require further understanding include:

1. *Modeling and control of insert-engagement induced surface pattern*

Insert engagement induced surface patterns are one major variation source as shown in Chapter 4. Such patterns are also affected by factors such as cutting conditions, cutter geometry, clamping conditions as well as workpiece material. For example, at higher cutting speed the impact of insert-engagement would be less severe. How the insert engagement induced patterns are affected has not been addressed. Future work will include experimental and theoretical study

of these effects and potential process adjustment method to suppress the insert engagement induced variation.

2. *Multi root cause diagnosis using multiscale surface shape*

On some occasions, certain process conditions could jointly contribute to both large and fine scale surface features. As such, the surface features at different scales are related to common process conditions. Understanding of this relationship would help improve surface quality control, process and system monitoring. Future work will fusion the information of large-scale features, fine-scale features, and cutting conditions to deliver enhanced surface modeling, process monitoring, and surface quality control. The framework is summarized in Figure 5-1.

3. *Process monitoring using multiscale surface shape*

Fine-scale surface features, such as roughness and waviness, and related process conditions have been studied deeply and broadly. But relationship between recently found large-scale surface patterns and process conditions as well as fine-scale surface features has not been studied well. Understanding of this relationship would help improving surface quality control, process and system monitoring (Figure 5-1).

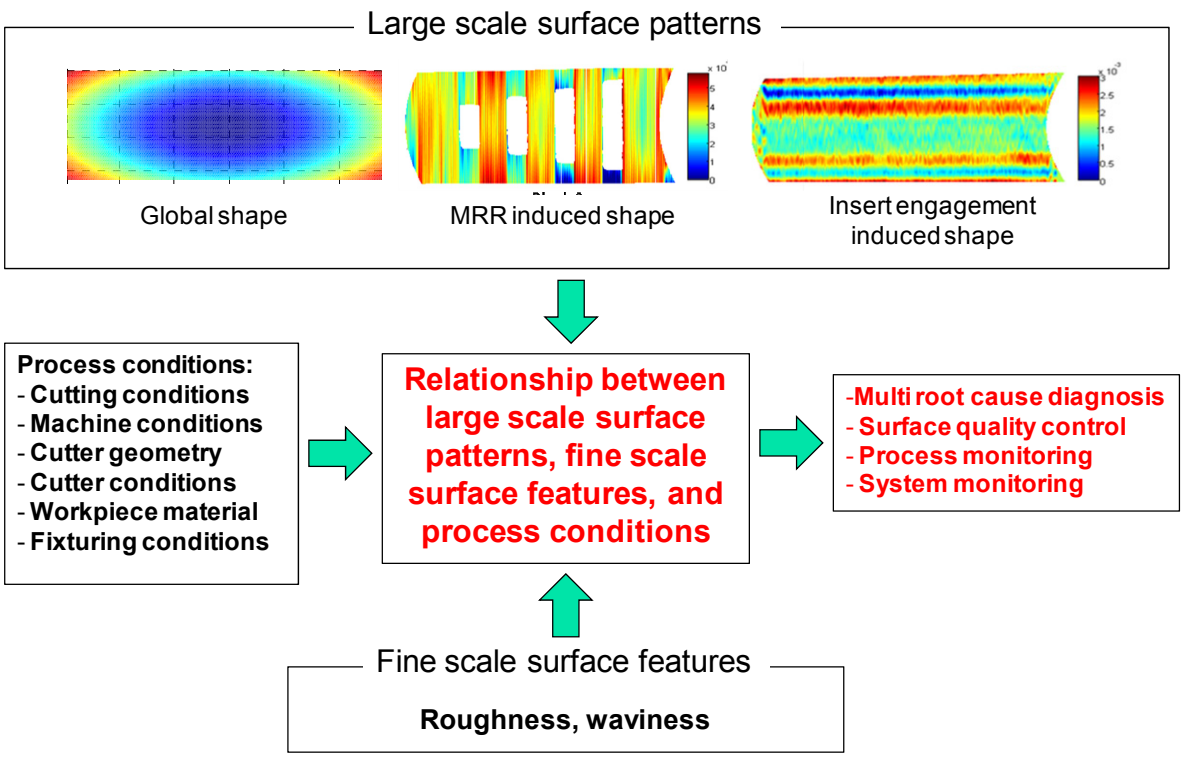

Figure 5-1 Study of integration of large-scale surface patterns, fine-scale surface features, and process conditions

4. *Multi-stage manufacturing system monitoring using HDM data*

For a multi-stage surface machining process, surface variation patterns can be attributed to variation sources from the current stage or previous stages. This thesis mainly discussed in detail how the within-stage variation sources in machining conditions cause the surface patterns; however, the interdependence between stages are not considered. Future work will focus on separation of the effects of within-stage and between-stage variation sources by modeling and analyzing the mixed surface patterns. As shown in Figure 5-2, the boxes in each row represent multiple samples on each operation and each column shows how one part goes through a N-stage process. The

proposed framework is summarized in Figure 5-2 which shows that the within-stage effect f(m) and between-stage effect g(i,j) will be identified and jointly considered for process monitoring and diagnosis.

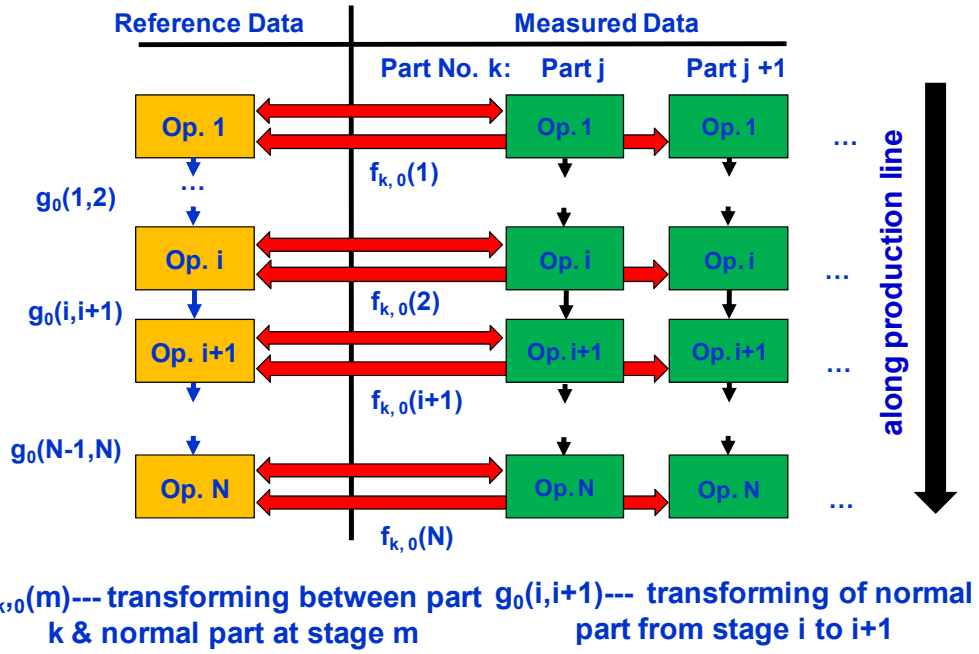

Figure 5-2 Multi-stage system monitoring

5. *Application of HDM to other machining processes*

The established methodology of surface characterization can be extended to other processes such as drilling, end milling, broaching, face turning, and micro-machining. Cylindrical bore surface inspection system, LHI, and micro LHI systems can be employed to capture variation patterns on different machined surfaces. Cutting force modeling will be conducted to extract surface variation patterns and new machining improvement approaches will be developed to reduce surface variations for these applications.

Bibliography

[1] Huynh, V. M., and Fan, Y., 1992, "Surface-Texture Measurement and Characterisation with Applications to Machine-Tool Monitoring," The International Journal of Advanced Manufacturing Technology, 7(1), pp. 2-10.

[2] Whitehouse, D. J., 1997, "Surface Metrology," Measurement Science and Technology, 8(9).

[3] Leith, E. N., 1997, "Overview of the Development of Holography," J. Image Sci. Technology, 41, pp. 201-204.

[4] Huang, Z., Shih, A. J., and Ni, J., 2006, "Laser Interferometry Hologram Registration for Three-Dimensional Precision Measurements," Transactions of the ASME, 128(4), pp. 887-896.

[5] Colosimo, B. M., and Senin, N., 2010, Geometric Tolerances: Impact on Product Design, Quality Inspection and Statistical Process Monitoring, Springer.

[6] Ertürk, A., Budak, E., and Özgüven, H. N., 2007, "Selection of Design and Operational Parameters in Spindle–Holder–Tool Assemblies for Maximum Chatter Stability by Using a New Analytical Model," International Journal of Advanced Manufacturing Technology, 47(9), pp. 1401-1409.

[7] Takeuchi, Y., and Sakamoto, M., 1964, "Analysis of Machining Error in Face Milling," Proceedings of the International Machine Tool Design and Research Conference.

[8] Franco, P., Estrems, M., and Faura, F., 2008, "A Study of Back Cutting Surface Finish from Tool Errors and Machine Tool Deviations during Face Milling," International Journal of Machine Tools and Manufature, 48(1), pp. 112–123.

[9] Schmitz, T. L., Couey, J., Marshb, E., Mauntler, N., and Hughes, D., 2006, "Runout Effects in Milling: Surface Finish, Surface Location Error, and Stability " International Journal of Machine Tools & Manufacture, 47(5), pp. 841-851.

[10] Kline, W. A., and DeVor, R. E., 1983, "The Effect of Runout on Cutting Geometry and Forces in End Milling," International Journal of Machine Tool Design and Research, 23(1-2), pp. 123-140

[11] F. Gu, S. G. K., and R. E. DeVor, 1997, "An Enhanced Cutting Force Model for Face Milling With Variable Cutter Feed Motion and Complex Workpiece Geometry," Journal of Manufacturing Science and Engineering 119(4A), p. 9.

[12] Huang, Y., and Hoshi, T., 2001, "Optimization of Fixture Design with Consideration of Thermal Deformation in Face Milling," Journal of Manufacturing Systems, 19(5), pp. 332-340.

[13] Chen, W., Ni, L., and Xue, J., 2008, "Deformation Control Through Fixture Layout Design and Clamping Force Optimization," International Journal of Advanced Manufacturing Technology 38(9-10), pp. 860–867.

[14] Kaya, N., 2006, "Machining Fixture Locating and Clamping Position Optimization Using Genetic Algorithms," Computers in Industry 57(2), pp. 112–120.

[15] Kulankara, K., Satyanarayana, S., and Melkote, S. N., 2002, "Iterative Fixture Layout and Clamping Force Optimization Using the Genetic Algorithm," Journal of Solar Energy Engineering 124(1), pp. 119–125.

[16] Deng, H., and Melkote, S. N., 2006, "Determination of Minimum Clamping Forces for Dynamically Stable Fixturing," International Journal of Machine Tools and Manufacture 46(7-8), pp. 847–857.

[17] Meter, E. C. D., 1995, "Min–max Load Model for Optimizing Machining Fixture Performance," Journal of Engineering for Industry 117(2), pp. 186–193.

[18] Korkut, I., and Donertas, M. A., 2007, "The Influence of Feed Rate and Cutting Speed in the Cutting Forces, Surface Roughness and Tool–Chip Contact Length During Face Milling," Materials and Design, 28(1), pp. 308–312.

[19] Baek, D. K., Ko, T. J., and Kim, H. S., 2001, "Optimization of Feedrate In A Face Milling Operation Using A Surface Roughness Model," International Journal of Machine Tools and Manufacture, 41(3), pp. 451–462.

[20] Ulutan, D., Alaca, B. E., and Lazoglu, I., 2007, "Analytical Modeling of Residual Stresses in Machining," Journal of Materials Processing Technology 2(3), pp. 77–87.

[21] Denkena, B., Boehnke, D., and deLeo, L., 2008, "Machining Induced Residual Stress In Structure Aluminum Parts," ProductionEngineer, 2(3), pp. 247–253.

[22] Andersson, C., Andersson, M., and Ståhl, J.-E., 2010, "Experimental Studies of Cutting Force Variation in Face Milling," International Journal of Machine Tools & Manufacture, 51(1), pp. 67-76.

[23] Fu, H. J., Devor, R. E., and Kapoor, S. G., 1984, "A Mechanistic Model for the Prediction of the Force System in Face Milling Operations," Transactions, ASME J. Eng. for Industry 106, pp. 81-88.

[24] Li, X. P., Zheng, H. Q., Wong, Y. S., and Nee, A. Y. C., 2000, "An Approach to Theoretical Modeling and Simulation of Face Milling Forces " Journal of Manufacturing Processes, 2(4), pp. 225-240.

[25] Ruzhong, Z., Wang, K. K., and Merchant, E., 1983, "Modelling of Cutting Force Pulsation in Face-Milling " CIRP Annals - Manufacturing Technology, 32(1), pp. 21-26.

[26] Wang, J.-J. J., Liang, S. Y., and Book, W. J., 1995, "Convolution Analysis of Milling Force Pulsation," ASME Journal of Engineering for Industry, 116(1), pp. 17-25.

[27] Hong-Tsu Young, P. M., and P.L.B. Oxley, 1994, "Predicting cutting forces in face milling " International Journal of Machine Tools and Manufacture, 34(6), pp. 771-783.

[28] Heikkala, J., 2000, "Determining of Cutting-Force Components in Face Milling," Journal of Materials Processing Technology, 52(1), pp. 1-8.

[29] Baek, D. K., Ko, T. J., and Kim, H. S., 1997, "A Dynamic Surface Roughness Model for Face Milling," Precision Engineering, 20(3), pp. 171-178.

[30] Montgomery, D., and Altintas, Y., 1991, "Mechanism of Cutting Force and Surface Generation in Dynamic Milling," Transactions of the ASME, 113(5), p. 160.

[31] Wu, D. W., 1989, "A New Approach of Formulating the Transfer Function for Dynamic Cutting Processes," ASME Journal of Engineering for Industry, 111, pp. 37-47.

[32] Smith, S., and Tlusty, J., 2008, "Stabilizing Chatter by Automatic Spindle Speed Regulation," CIRP Annals - Manufacturing Technology, 41(1), pp. 433–436.

[33] Tarng, Y. S., and Li, T. C., 1994, "The Change of Spindle Speed for the Avoidance of Chatter in End Milling," Journal of Materials Processing Technology, 41(2), pp. 227–236.

[34] Huang, Y., and Hoshi, T., 2000, "Improvement of Flatness Error in Milling Plate-Shaped Workpiece by Application of Side-Clamping Force," Precision Engineering, 24(4), pp. 364–370.

[35] 2003 Surface Texture, Surface Roughness, Waviness and Lay: ASME B46.1-2002 American Society of Mechanical Engineers

[36] Liao, Y., Stephenson, D. A., and Ni, J., 2009, "Assessment of Tool Wear Based on Surface Texture Parameters," ASME 2009 International Manufacturing Science and Engineering Conference, 2, pp. 463-470.

[37] Wong, C. B. a. Y. S., 2001, "Surface Texture Indicators of Tool Wear - A Machine Vision Approach " The International Journal of Advanced Manufacturing Technology, 17(6), pp. 435-443.

[38] D. Jaumea, M. V., A. Raultb and A. Moisanc, 1990, "A Model-Based Diagnosis in Machine Tools: Application to the Milling Cutting Process " CIRP Annals - Manufacturing Technology, 39(1), pp. 443-446.

[39] Gu, F., Melkote, S. N., Kapoor, S. G., and DeVor, R. E., 1997, "A Model for the Prediction of Surface Flatness in Face Milling," Journal of Manufacturing Science and Engineering 119(4A), p. 9.

[40] Liao, Y. G., and Hu, S. J., 2001, "An Integrated Model of a Fixture-Workpiece System for Surface Quality Prediction," International Journal of Advanced Manufacturing Technology, 17(11), pp. 810-818.

[41] Chang, H.-K., Kim, J.-H., Kim, I. H., Jang, D. Y., and Han, D. C., 2007, "In-Process Surface Roughness Prediction Using Displacement Signals from Spindle Motion," International Journal of Advanced Manufacturing Technology, 47(6), pp. 1021–1026.

[42] Tai, B. L., David A. Stephenson, and Shih, A. J., 2010, "Improvement of Surface Flatness in Face Milling Based on 3-D Holographic Laser Metrology," International Journal of Machine Tools and Manufacture, 51(6), pp. 483–490.

[43] Wilkinson, P., Reuben, R. L., Jones, J. D. C., Barton, J. S., Hand, D. P., Carolan, T. A., and Kidd, S. R., 1997, "Surface Finish Parameters as Diagnostics of Tool Wear in Face Milling " Wear, 205(1-2), pp. 47-54.

[44] Waldorf, D. W., S. G. Kapoor, and R. E. DeVor, 1992, "Automatic Recognition of Tool Wear on a Face Mill Using a Mechanistic Modeling Approach," International Journal of Wear, 157, pp. 305-323.

[45] Takata, S., Nakajima, T., Ahn, J. H., and Sata, T., 1987, "Tool Breakage Monitoring by Means of Fluctuations in Spindle Rotational Speed," CIRP Annals - Manufacturing Technology, 3(1), pp. 49–52.

[46] Jayaram, S., S. G. Kapoor, and R. E. DeVor, 1997, "A Model-Based Approach for Detection of Process Faults in the Face Milling Process," Transactions of the North American Manufacturing Research Institution of SME, XXV.

[47] Camelio, J., Hu, S. J., and Zhong, W., 2004, "Diagnosis of Multiple Fixture Faults in Machining Processes Using Designated Component Analysis," Journal of Manufacturing Systems, 23(4), pp. 309-315.

[48] Sutherland, J. W., and DeVor, R. E., 1986, "Improved Method for Cutting Force and Surface Error Prediction in Flexible End Milling Systems," ASME Journal of Engineering for Industry, 108(4), pp. 269-279.

[49] Raja, J., Muralikrishnan, B., and Fu, S., 2002, "Recent Advances in Separation of Roughness, Waviness and Form," Precision Engineering, 26(2), pp. 222-235.

[50] Tai, B. L., Wang, H., Nguyen, H., Hu, S. J., and Shih, A., 2012, "Surface Variation Reduction for Face Milling Based on High Definition Metrology," 2012 ASME International Manufacturing Science and Engineering Conference, No. 7208.

[51] Smith, G. T., 1989, Advanced Machining, Springer-Verlag, New York.

[52] Nguyen, H. T., Wang, H., and Hu, S. J., 2011, "Characterization of Cutting Force Induced Surface Shape Variation Using High-Definition Metrology," 2012 ASME International Manufacturing Science and Engineering Conference, No. 7312.

[53] Takataa, S., Nakajimab, T., Ahnc, J. H., and Satad, T., 1987, "Tool Breakage Monitoring by Means of Fluctuations in Spindle Rotational Speed," CIRP Annals - Manufacturing Technology, 36(1), pp. 49-52.

[54] Sridhar Sastry, Shiv G. Kapoor, and DeVor, R. E., 1999, "Compensation of Progressive Radial Run-Out in Face-Milling by Spindle Speed Variation," international Journal of Machine Tools & Manufacture, 40(8), pp. 1121–1139.

[55] Chu, C. N., Kim, S. Y., Lee, J. M., and Kim, B. H., 1997, "Feed-rate Optimization of Ball-end Milling Considerating Local Shape Features," CIRP Annals-Manufacturing Technology, 46(1), pp. 433-436.

[56] Lim, E. M., and Meng, C. H., 1997, "Integrated Planning for Precision Machining of Complex Surface. Part I: Cutting Path and Federate Optimization," International Journal of Machine Tools and Manufacture, 37(1), pp. 61-75.

[57] Ko, J. H., and Cho, D. W., 2004, "Feed Rate Scheduling Model Considering Transverse Rupture Strength of Tool for 3D Ball-end Milling," International Journal of Machine Tools and Manufacture, 44(10), pp. 1047-1059.

[58] De Meter, M. C., 2004, "Min-Max Load Model for Optimzing Machining Fixture Performance," ASME Journal of Engineering for Industry, 117(2), pp. 186-193.

[59] De Meter, M. C., 1998, "Fast Support Layout Optimization," International Journal of Machine Tools & Manufacture, 38(10-11), pp. 1221-1239.

[60] Nee, A. Y. C., Senthil Kumar, A., and Tao, Z. J., 2000, "An Intelligent Fixture with a Dynamic Clamping Scheme," Proceedings of the Institution of Mechanical Engineers, Part B: Journal of Engineering Manufacture, 214(3), pp. 183-196.

[61] Kulankara, K., Satyanarayana, S., and Melkote, S. N., 2002, "Iterative Fixture Layout and Clamping Force Optimization Using the Genetic Algorithm," Journal of Manufacturing Science and Engineering, Transactions of the ASME, 124(1), pp. 119-125.

[62] Deng, H., and Melkote, S. N., 2006, "Determination of Minimum Clamping Forces for Dynamically Stable Fixturing," International Journal of Machine Tools and Manufacture, 46(7-8), pp. 847-857.

[63] Kaya, N., 2006, "Machining Fixture Locating and Clamping Position Optimization Using Genetic Algorithms," Computers in Industry, 57(2), pp. 112-120.

[64] Chen, W., Ni, L., and Xue, J., 2008, "Deformation Ccontrol Through Fixture Layout Design and Clamping Force Optimization," International Journal of Advanced Manufacturing Technology, 38(9-10), pp. 860-867.

[65] Huang, Y., and Hoshi, T., 2000, "Improvement of Flatness Error in Milling Plate-Shaped Workpiece by Application of Side-Clamping Force," Precision Engineering, 24(4), pp. 364-370.

[66] Tai, B. L., Stephenson, D. A., and Shih, A. J., 2011, "Improvement of Surface Flatness in Face Milling Based on 3-D Holographic Laser Metrology," International Journal of Machine Tools and Manufacture, 51(6), pp. 483-491.